


RESEARCH ARTICLE

Open Access



Evaluation of cloud and precipitation processes in regional and global models with ULTIMATE (ULTra-slte for Measuring Atmosphere of Tokyo metropolitan Environment): a case study using the dual-polarization Doppler weather radars

Masaki Satoh^{1*} , Shuhei Matsugishi¹, Woosub Roh¹, Yasutaka Ikuta², Naomi Kuba¹, Tatsuya Seiki³, Tempei Hashino⁴ and Hajime Okamoto⁵

Abstract

We describe a collaborative analysis study involving numerical models and observation data for the Tokyo metropolitan area called the ULTra-slte for Measuring Atmosphere of Tokyo Metropolitan Environment (ULTIMATE) project. It evaluates cloud microphysics schemes of numerical models using extensive observation data for the Tokyo area. We have access to various remote sensing and in situ data for the Tokyo area for operational and research purposes, particularly by enhancing observations for ground validation of the EarthCARE satellite, which is set to launch in 2023. This study focuses on using the dual-polarization Doppler weather radar, operated by the Japan Meteorological Agency. In terms of numerical models, we use and compare multi-models with single-moment (SM) and double-moment (DM) cloud microphysics schemes; the global non-hydrostatic model, Non-hydrostatic ICosahedral Atmospheric Model (NICAM) and the two regional models with A System based on a Unified Concept for Atmosphere (ASUCA) and Scalable Computing for Advanced Library and Environment (SCALE) are used. In particular, because NICAM can be used as both a global and a regional model, we can immediately test the improved scheme on a global scale for its effect on climatology and the evaluation of climate sensitivity. This paper introduces the methodology for evaluating numerical models by the dual-polarization radar using the observation simulator and compares numerical model results with observations. In particular, we evaluate the simulated rain in the lower level near the ground and the large ice particles just above the melting level. The simulation with NICAM-DM reproduces the comparable polarimetric radar characteristics of rain as the observation. However, the simulations with NICAM-SM and ASUCA-SM show larger raindrop sizes in stronger rain areas compared to the observation. For the larger ice particles just above the melting level around 4 km, NICAM-DM and ASUCA-SM overestimate particle sizes of graupel or snow, while NICAM-SM has a similar size of the ice particles. In future studies, we will use the present results to improve the cloud microphysics scheme, which will be tested on a global model.

*Correspondence: satoh@aori.u-tokyo.ac.jp

¹ Atmosphere and Ocean Research Institute, The University of Tokyo, 5-1-5 Kashiwanoha, Kashiwa, Chiba 277-8564, Japan
Full list of author information is available at the end of the article

Keywords: ULTIMATE, Cloud microphysics, EarthCARE, Polarimetric radar, Regional and global models

1 Introduction

Atmospheric numerical models are used for weather forecasts and climate projections, such as daily weather forecasting and future climate change. Precipitation and the atmospheric energy balance in these models depend heavily on representing cloud microphysical processes. To improve the prediction accuracy of extreme atmospheric events such as heavy rainfalls and typhoons, it is necessary to accurately predict convective clouds by representing the formation of clouds and precipitations. The projection of future temperature change in climate models (e.g., climate sensitivity; Sherwood et al. 2020) is also greatly affected by the representation of cloud microphysical processes. However, cloud schemes in these weather and climate models are highly uncertain and must be validated by various observational data.

Many studies have validated numerical models using satellite data, particularly from the satellite simulator approach (Masunaga et al. 2010; Bodas-Salcedo et al. 2011). The atmospheric general circulation models (hereafter referred to as GCMs) used in the Cloud Feedback Model Intercomparison Project (CFMIP; Webb et al. 2017) were evaluated by using the CFMIP Observation Simulator Package (COSP; Bodas-Salcedo et al. 2011) to contribute to the Coupled Model Intercomparison Project Phase 6 (CMIP6; Eyring et al. 2016). Recently, higher-resolution global storm-resolving models (hereafter referred to as GSRMs), in which cloud microphysics schemes are used to simulate convective clouds explicitly without using cumulus parameterization, have been used more widely for weather and climate simulations (Sato et al. 2019). A dedicated satellite simulator package has been used to evaluate GSRMs to consider more consistency among sensor simulators (Hashino et al. 2013; Sato et al. 2016). Roh et al. (2021) compared the vertical cloud profiles from the simulated data of the first inter-comparison experiment for GSRMs, called the Dynamics of the Atmospheric general circulation Modeled On Non-hydrostatic Domains (DYAMOND; Stevens et al. 2019), and found a wide diversity of profiles among the models. Therefore, to improve the cloud microphysics schemes used in GSRMs, simulated clouds and precipitation should be more carefully evaluated using observation.

Some types of GSRMs can be used as seamless models with a common dynamical core and physics schemes for regional and global configurations; examples of such GSRMs are the Non-hydrostatic ICosahedral Atmospheric Model (NICAM; Tomita and Sato 2004; Sato et al. 2008, 2014), ICosahedral Non-hydrostatic model

(ICON; Zängl et al. 2014), Model for Prediction Across Scales (MPAS; Skamarock et al. 2012), System for High-resolution prediction on Earth-to-Local Domains (SHiELD; Harris et al. 2020), and System for Atmospheric Modeling (SAM; Khairoutdinov et al. 2022). NICAM can simulate a global atmosphere using a quasi-uniform-grid system (Tomita et al. 2001) and simulate local regions at high resolution using a stretched grid system (hereafter referred to as stretch-NICAM; Tomita 2008; Uchida et al. 2016; 2017). Several studies have evaluated clouds simulated by NICAM by comparing them with satellite data using satellite simulators (Masunaga et al. 2008; Sato et al. 2010; Kodama et al. 2012; Hashino et al. 2013, 2016; Roh and Sato 2014; Roh et al. 2017, 2018, 2020; Matsui et al. 2016). In particular, Roh and Sato (2014) simulated cumulus clusters with stretch-NICAM focused on the tropics. They compared the simulated results with observations from the Tropical Rainfall Measuring Mission (TRMM) satellite to improve the cloud microphysics scheme. Hashino et al. (2013) evaluated model results using a satellite simulator, called the Joint Simulator for Satellite Sensors, to calculate satellite signal values from numerical model results and compare them directly with the satellite observations by CloudSat and Cloud-Aerosol Lidar and Infrared Pathfinder Satellite Observations (CALIPSO). In the High Resolution Model Intercomparison Project (HighResMIP; Haarsma et al. 2016) experiment of CMIP6 using NICAM (Kodama et al. 2021), the cloud microphysics scheme developed by Roh and Sato (2014) was applied to the global simulation.

Furthermore, Roh et al. (2020) evaluated simulated lower clouds in the Southern Ocean using stretch-NICAM with lidar observation data by the Cloud Aerosol Lidar with Orthogonal Polarization (CALIOP) onboard CALIPSO. Based on these results, Seiki and Roh (2020) improved the cloud microphysics scheme of NICAM to reproduce supercooled water in the Southern Ocean more realistically. Their improvement of the cloud microphysics scheme is essential for future climate experiments using NICAM for the global domain (Noda et al. 2021).

Previous studies evaluating and improving cloud microphysics schemes of global atmospheric models have mainly used satellite observation data. However, there are more types and volumes of remote sensing data in ground-based observations than in satellite observations. Therefore, we expect that the cloud microphysics schemes can be further evaluated and improved by investigating clouds and precipitation using

ground-based observation data. Ground-based observation has been used mainly to evaluate regional numerical models. Recently, however, it has become possible to evaluate both regional and global models using ground-based observations due to developing a seamless model approach for GSRMs that use a common cloud microphysics scheme for regional and global models.

To validate and improve regional and global numerical models using various observational data in a local area, we developed a research framework called ULTIMATE (ULtra-slte for Measuring Atmosphere of Tokyo metropolitan Environment), which uses intensive observation data in the Tokyo metropolitan region for model evaluations. The goal of ULTIMATE is to improve the accuracy of numerical models through validation and improvement of their cloud microphysics to achieve better regional and global simulations. Our research framework ULTIMATE aims to assess cloud microphysical processes in a unified approach in more detail by using various types of ground-based observation data, which have not been fully exploited in previous studies of GSRMs.

This paper introduces ULTIMATE as a research framework for validating and improving a numerical model that seamlessly computes regional and global clouds and presents the first result of ULTIMATE. This project is a part of the ground-based observation evaluation program planned for the EarthCARE satellite (Illingworth et al. 2015), scheduled for launch in 2023. In ULTIMATE, numerical models can be verified and improved by comparing simulated results with ground-based and satellite observations. Here, we describe our specific method for evaluating numerical models using observations from the dual-polarization Doppler weather radar installed by the Japan Meteorological Agency (JMA).

2 Methods/experimental

2.1 Observations at the Kanto region ultra-site

In the Kanto region, various remote sensing observation networks have been established by operational and research organizations. Thus, the Kanto region has the characteristics of an observational “ultra-site” that surpasses so-called supersites. Previous research projects in the Kanto region have combined observations and numerical models. The Tokyo Metropolitan Area Convection Study for Extreme Weather Resilient Cities (TOMACS) has been conducted since 2010 to elucidate the mechanisms behind local high-impact weather in urban areas, improve nowcasting and forecasting techniques, and share high-resolution weather information to end-users through social experiments (Misumi 2018; Misumi et al. 2019). In the summers of 2020 and 2021, a RIKEN team conducted a real-time demonstration of ultra-fast precipitation forecasting for the Kanto

region using the Multi-Parameter Phased Array Weather Radar (MP-PAWR) installed in Saitama Prefecture, Japan (Miyoshi et al. 2020). Following these previous studies, ULTIMATE also targets the Kanto region. In ULTIMATE, we focus on evaluating cloud and precipitation processes, the most uncertain components in numerical models.

ULTIMATE utilizes a series of observational data prepared as ground validations for the satellite mission EarthCARE (Illingworth et al. 2015). The observation data used for ULTIMATE are introduced in “Appendix 1.” Figure 1 shows an overview of these observation data networks. These observation datasets make it possible to collectively perform a comprehensive spatiotemporal analysis of cloud precipitation systems, such as severe convective systems in the Kanto region. We can use these datasets for the validation and improvement of numerical models.

Among various observation data, this study uses the JMA’s C-band dual-polarization Doppler radar for airport weather at the Haneda and Narita airports. The basic specifications of the Haneda and Narita radars are described in Table 1 and are referred to Tsukamoto et al. (2016) and Umehara et al. (2021).

Similar intensive projects with observation-model collaborations, including polarimetric radars, are underway in other countries. The German Priority Programme, called Polarimetric Radar Observations meet Atmospheric Modelling (PROM), which started in 2019, aims to synergize polarimetric radar observations and atmospheric models to understand cloud and precipitation processes better and to improve their representation in numerical models (Trömel et al. 2021). In the USA, the BiLateral Operational Storm-Scale Observation and Modeling (BLOSSOM) Project has been proposed (Matsui et al. 2019a).

Using observation simulators for evaluating numerical models using data from polarimetric radars is becoming a standard approach (Matsui et al. 2019b, 2020; Shrestha et al. 2022). Intensive research has been conducted on collaborating polarimetric radar observations and numerical modeling in regional model studies. Jung et al. (2010) developed a polarimetric radar simulator and applied it to the simulation data of a supercell storm. They suggest that two- or higher-moment microphysics schemes can adequately describe certain important microphysical processes comparable to the observed polarimetric parameters. Snyder et al. (2017a, 2017b) further applied the simulator to supercell experimental results with a three-moment microphysics scheme and described evolutions of the polarimetric parameters. Ryzhkov et al. (2011) applied the simulator to a more detailed spectral bin model result. Putnam et al. (2017)

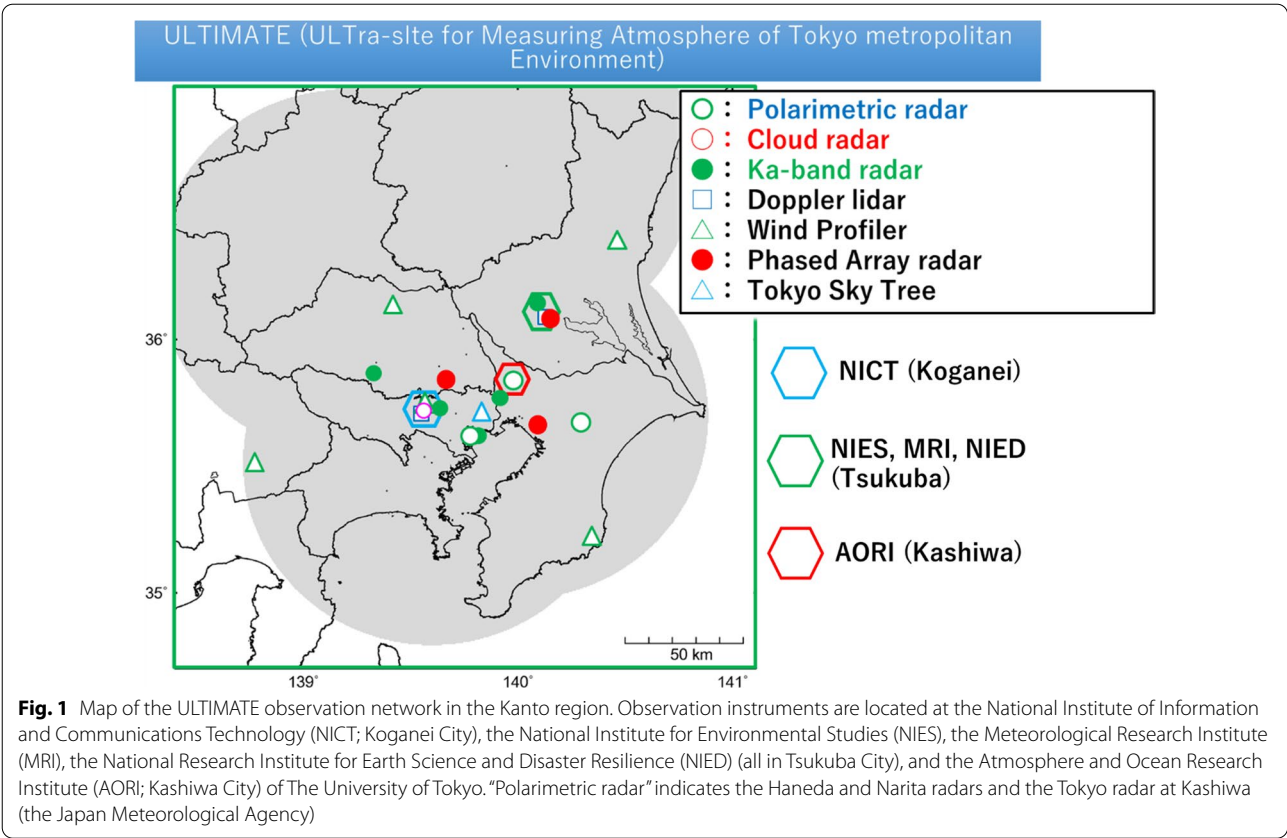


Table 1 Basic specifications of the Haneda and Narita radars (Tsukamoto et al. 2016; Umehara et al. 2021)

Transmitting frequency	C-band (5330 MHz at the Haneda radar and 5335 MHz at the Narita radar)
Beam width	< 0.7° (7-m-diameter parabolic antenna)
Pulse width	1 μs (range < 12 km), 64 μs (range ≥ 12 km)
Azimuth spacing	0.7°
Range gate spacing	150 m
Observable range radius	120 km
Observation frequency	A volume scan (including 15 PPIs and an RHI) updates every 5 min
Elevation angles of PPI	0.7°, 17.0°, 12.5°, 0.7°, 9.2°, 6.9°, 5.1°, 0.7°, 3.8°, 2.8°, 2.1°, 0.7°, 1.5°, 1.1°, 0.7°
Azimuth angles of RHI	Haneda: 329.8° to 149.8° and 239.8° to 59.8° Narita: 149.5° to 329.5° and 239.5° to 59.5° The two orthogonal planes are 5 min alternatively scanned
Transmission mode	Simultaneous transmit and receive (STAR) mode

systematically compared various cloud microphysics schemes by applying the simulator to simulations for a mesoscale convective system (MCS) and supercell cases. These studies are based on regional models and applications to specific weather phenomena such as MCS and supercell cases. These studies highlight the polarimetric radar characteristics in MCS and supercell cases and the importance of a multi-moment scheme to represent polarimetric parameters such as by a size-sorting effect

of hydrometeors. Bringi et al. (2020) proposed how to improve rain and riming processes of cloud microphysics schemes using polarimetric radar observations of a hurricane. Multi-frequency Doppler radar observations are also used to improve snow aggregation representation in a cloud microphysics scheme (Karrer et al. 2021). These ground-observation-modeling studies are uniquely important because of the characterization of weather systems in each area, even though thermodynamic

Table 2 Overview of all simulations

Model	Mesh size	Initial condition	Cloud microphysics scheme
ASUCA	1 km	Meso-scale Analysis	MP2003
NICAM-NSW6	1.4 km*	ERA5 reanalysis	NSW6
NICAM-NDW6	1.4 km*	ERA5 reanalysis	NDW6
SCALE-NSW6	1 km	Meso-scale Analysis	NSW6
SCALE-NDW6	1 km	Meso-scale Analysis	NDW6

*For NICAM-NSW6 and NICAM-NDW6, the minimum mesh size of the stretched grid is provided

conditions primarily determine cloud microphysics processes (Hashino et al. 2013). Among the weather systems observed in the Kanto area, we focus in this study on severe convective systems associated with an extratropical cyclone. As a companion study, Ikuta et al. (2022) analyzed the typhoon FAXAI (2019) as part of ULTIMATE. Such severe convective systems are frequently observed in the Kanto region, indicating the uniqueness of the observation of ULTIMATE.

2.2 Numerical models

We use three numerical models in this study, as shown in Table 2. First, we use NICAM, with which we can seamlessly simulate both domain-scale and global experiments in the same model (Sato et al. 2014). NICAM can directly resolve MCSs over the globe with a quasi-uniform horizontal grid spacing (of a few kilometers). In addition, NICAM can be used as a regional model to represent local mesoscale weather systems in detail by using a stretched grid model (stretch-NICAM) in which

the mesh is concentrated in a target region such as the Kanto region. NICAM uses the same dynamical and physical schemes and common program code for global and regional simulations. It is possible to switch between the global and regional models by changing the model configuration. Thus, the cloud microphysics schemes developed for global cloud-resolving simulations with NICAM (Sato et al. 2014) can be tested for both global and regional systems. In the present study, we conduct regional simulations using stretch-NICAM and evaluate the results by comparing them with ground-based observation data. These results can be used in the global version of NICAM to study global cloud precipitation processes and climatology and clarify their impact on climate sensitivity and global cloud distribution.

In this study, we use two types of bulk cloud microphysics schemes in stretch-NICAM simulations: NICAM single-moment bulk cloud microphysics with six water categories (NSW6) and NICAM double-moment bulk cloud microphysics with six water categories (NDW6; Seiki and Nakajima 2014; Seiki et al. 2014; 2015). NSW6 was proposed by Tomita (2008) and was improved by Roh and Sato (2014) by comparing it with satellite observation data. Clouds simulated by NICAM with NSW6 have been evaluated by Roh et al. (2017) and Kodama et al. (2012, 2021). NDW6 was introduced by Seiki and Nakajima (2014) and was evaluated by Seiki et al. (2014, 2015). The development of the two schemes is summarized in Sato et al. (2018). We assess the results of the regional experiment by stretch-NICAM using the observation data from the Kanto ultra-site to improve the cloud microphysics schemes. As for the horizontal resolution, we obtain

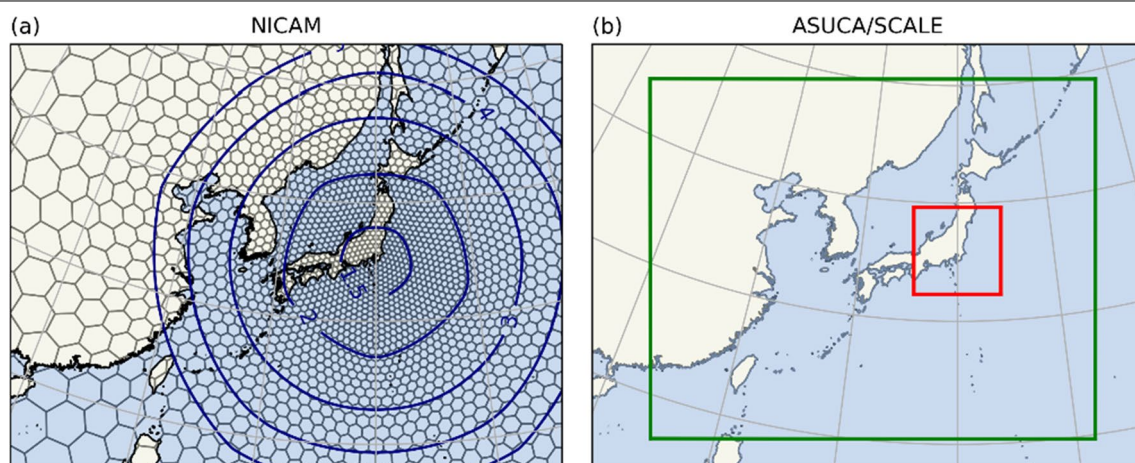


Fig. 2 **a** Schematic image of the grid structure of stretch-NICAM. The grid structure for g-level 4 is shown for readability. The actual grid used for the simulation is at g-level 9, whose grid can be obtained by subdividing the grid of g-level 4. Navy contours show the areas of the grid interval of g-level 9 at 1.5, 2, 3, 4, and 5 km. **b** The calculation domains for ASUCA for the 5 km mesh model (green) and the 1 km mesh model (red)

the minimum grid spacing of 1.4 km by setting the grid partition to level 9 (g-level 9) and the stretch factor to 100 in stretch-NICAM (Fig. 2, left). Initial values for the simulations were obtained from the European Centre for Medium-Range Weather Forecasts (ECMWF) Reanalysis v5 (ERA5; Hersbach et al., 2020).

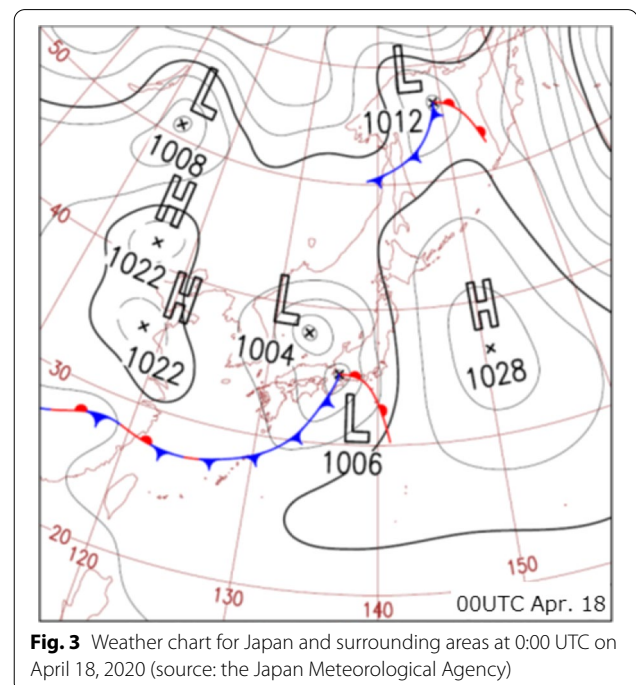
It is possible to perform numerical simulations using other high-resolution models for an area limited to the Kanto region. We use the JMA's regional domain model, ASUCA (A System based on a Unified Concept for Atmosphere; Japan Meteorological Agency 2019) and SCALE (Scalable Computing for Advanced Library and Environment) developed by RIKEN (Nishizawa et al. 2015; Sato et al. 2015) for comparison. For ASUCA, we use the cloud microphysics scheme MP2003, described in Ikuta et al. (2021). For SCALE, the same schemes as in NICAM are used for this study: NSW6 and NDW6. In principle, comparing experiments with multi-models can reveal the differences and uncertainties of cloud microphysics schemes in these numerical models. We should also note that the differences in other factors, including the dynamical cores, affect representations of clouds and precipitation; this is revealed by comparing results from NICAM and SCALE. For ASUCA and SCALE, we conduct experiments with a grid spacing of 1 km. The simulation domain of the two models is the same and covers the whole area of the Kanto region (Fig. 2, right). For ASUCA, we first simulate the Japan region at a resolution of 5 km, using the same settings as the Meso-Scale Model (MSM) of JMA (Japan Meteorological Agency 2019). The 5 km initial value is from the Meso-scale Analysis of JMA, and the boundary values are from the JMA global model forecast. For SCALE, we used the results of ASUCA with a resolution of 5 km as the initial and boundary values. We integrated the Kanto region over an area almost identical to that used in ASUCA, with a resolution of 1 km. The initial value for all models was set to 00:00 on April 18, 2020, and a 12-h time evolution was simulated in the models.

2.3 Analysis method

We use the observation simulator, POLARRIS (POLArimetric Radar Retrieval and Instrument Simulator) (Matsui et al. 2019b, 2020) to evaluate experimental results by the data from the dual-polarization Doppler weather radar. POLARRIS is implemented in the Joint Simulator for Satellite Sensors (hereafter referred to as J-Sim; Hashino et al. 2013; Sato et al. 2016), and the experimental results are processed with POLARRIS. POLARRIS comprises the forward simulator (POLARRIS-f) and the inverse retrieval and diagnostic components (iPOLARRIS). POLARRIS-f calculates the polarimetric radar parameters (horizontally polarized reflectivity Z_{th} [dBZ];

differential reflectivity Z_{dr} [dB]; specific differential phase K_{dp} [$^{\circ}$ km $^{-1}$]; and copolar correlation coefficient ρ_{hv}). These values are directly compared to observed values from the dual-polarization Doppler weather radar. iPOLARRIS is based on the Colorado State University (CSU) radar Hydrometeor Identification (HID) (e.g., Dolan et al. 2013; Dolan and Rutledge 2009). Ten categories are allowed in the HID: Drizzle, Rain, Ice Crystals, Aggregates, Wet Snow, Vertical Ice, Low-Density Graupel (LD Graupel), High-Density Graupel (HD Graupel), Hail, and Big Drops.

The parameters of axis ratio and orientation angle distributions of ice particles used for POLARRIS are referred to in Table 1 of Matsui et al. (2019a, b). We use the setting of “MA18” following Matsui et al. (2019a, b). In simulations, the cloud microphysics schemes assume their characteristics from the shapes of ice particles. For example, the cloud ice of NDW6 is assumed to be non-spherical. However, snow and graupel are assumed to be spherical in all the simulations used in this study. We note that the parameters used for the NICAM simulations are not necessarily consistent with those in J-Sim; we can test more detailed assumptions such as shape information of ice particles in J-Sim (Roh and Sato 2018). Matsui et al. (2020) stated that the polarimetric parameters above the melting layer comprise significant uncertainties due to the assumption in POLARRIS-f. In addition, the bright band is not well represented by POLARRIS-f because the polarization parameters cannot be calculated for melted particles which should be diagnosed by a bright



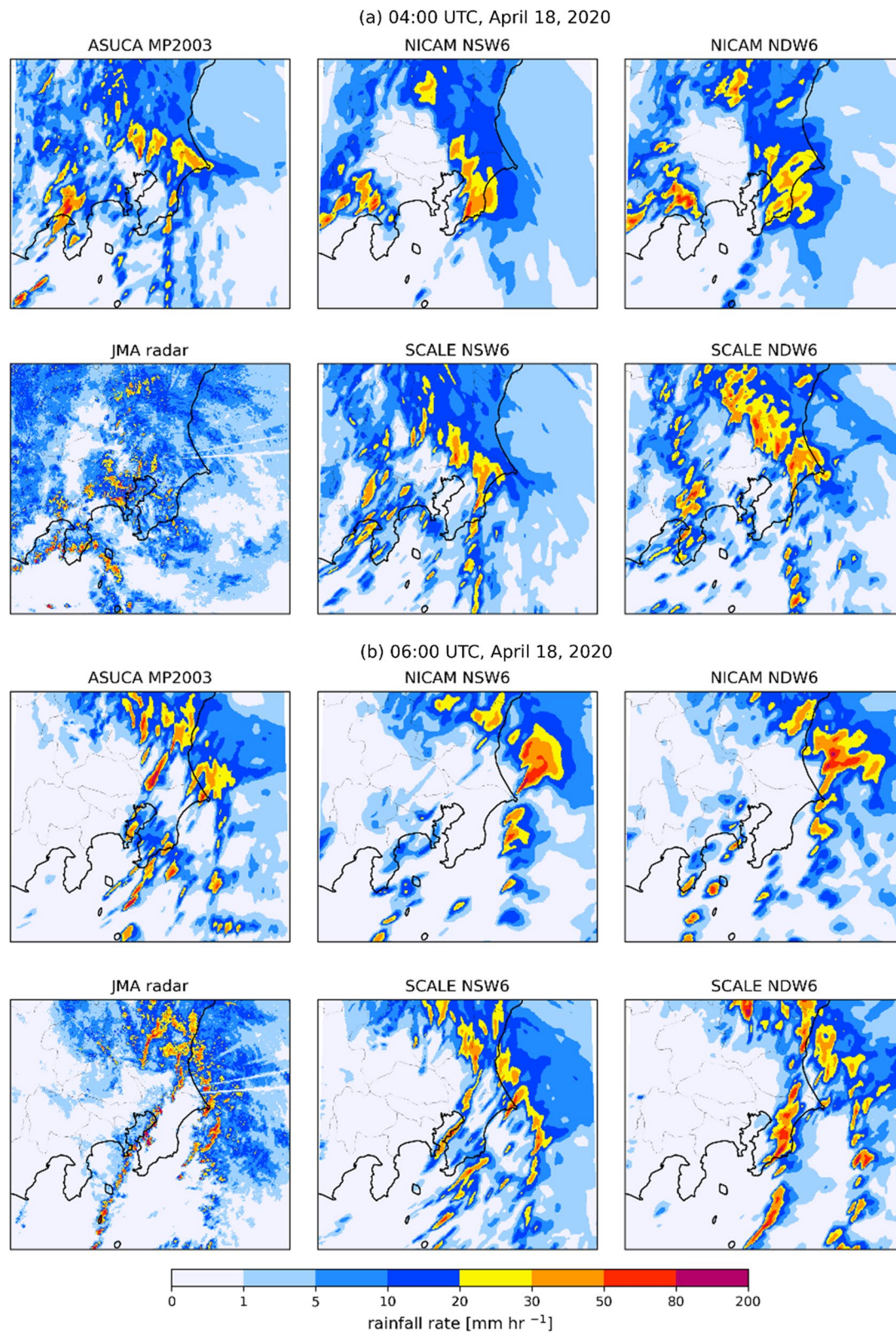


Fig. 4 Comparison of numerical simulations of rainfall distributions at **a** 04:00 UTC (top 6 panels) and **b** 06:00 UTC (bottom 6 panels) on April 18, 2020. In each group of 6 panels; Top row, from left to right: ASUCA 1-km grid, NICAM-NSW6 1.4-km grid, NICAM-NDW6 1.4 km grid; Bottom row, from left to right: radar observation rainfall rate, SCALE-NSW6 1 km grid, and SCALE-NDW6 1 km grid

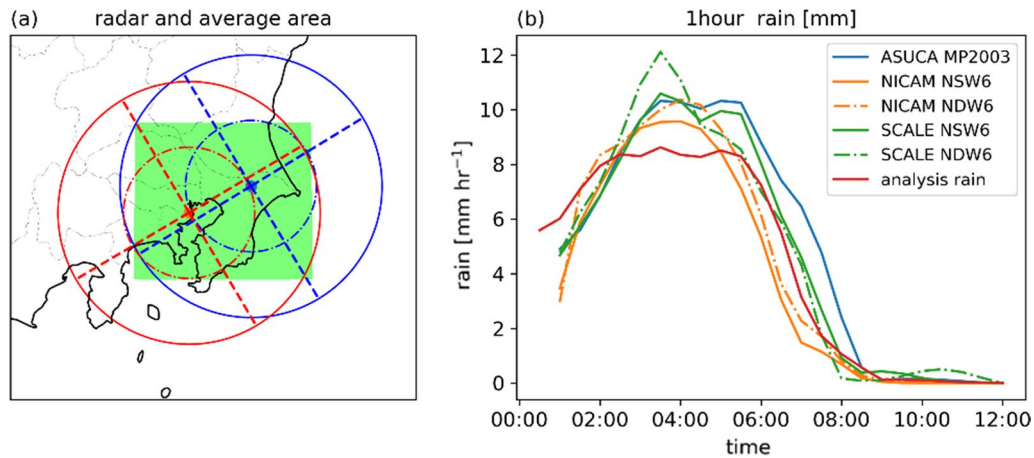


Fig. 5 **a** Distance circles with a radius of 60 km (dashed circle) and 120 km (solid circle) from the Haneda (red) and Narita (blue) radars. The dotted lines indicate the RHI (Range–Height Indicator) observation lines. Green shading shows the area used to compare rainfall and mass concentrations. **b** Temporal variation in 1-h rainfall amount from 00:00 to 12:00 UTC on April 18, 2020, in ASUCA (blue), NICAM-NSW6 (solid orange), NICAM-NDW6 (dotted orange), SCALE-NSW6 (solid green), SCALE-NDW6 (dotted green), and observed rainfall amount (red)

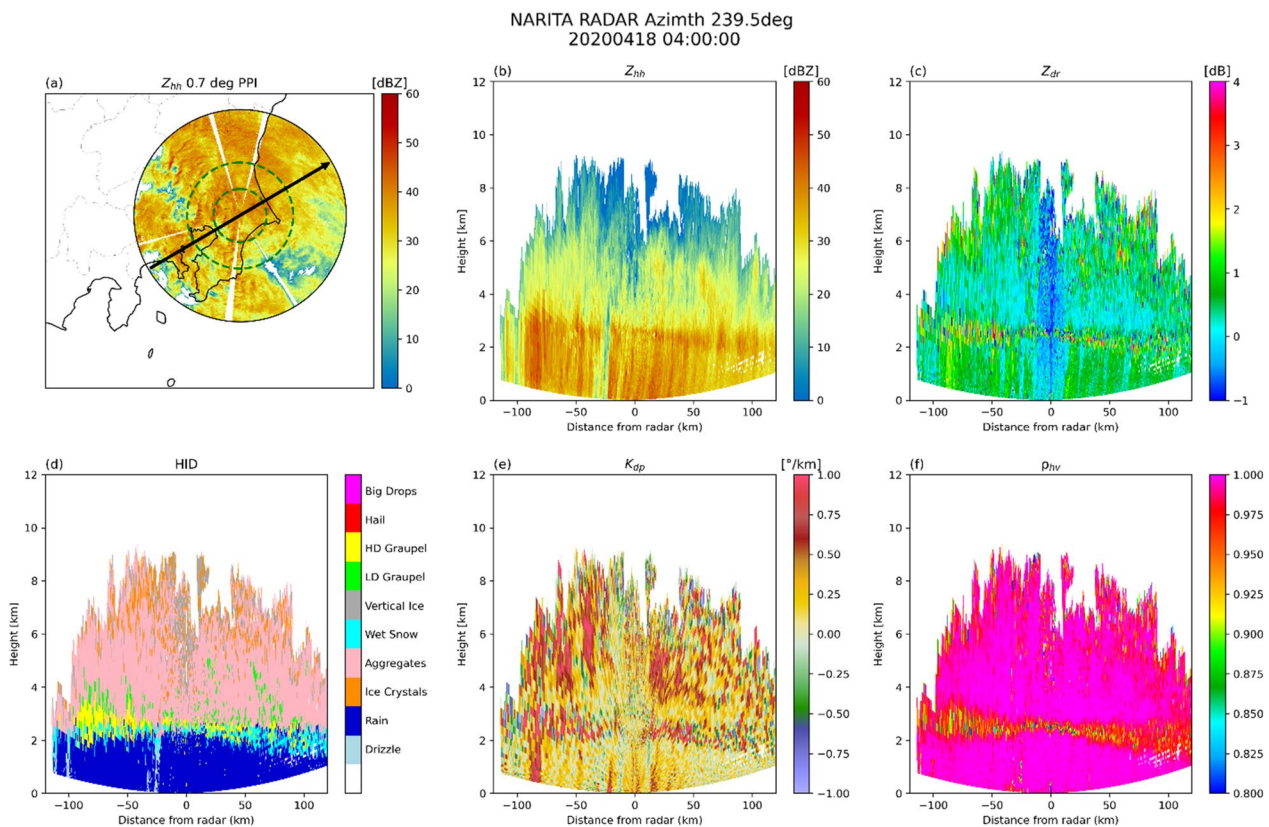
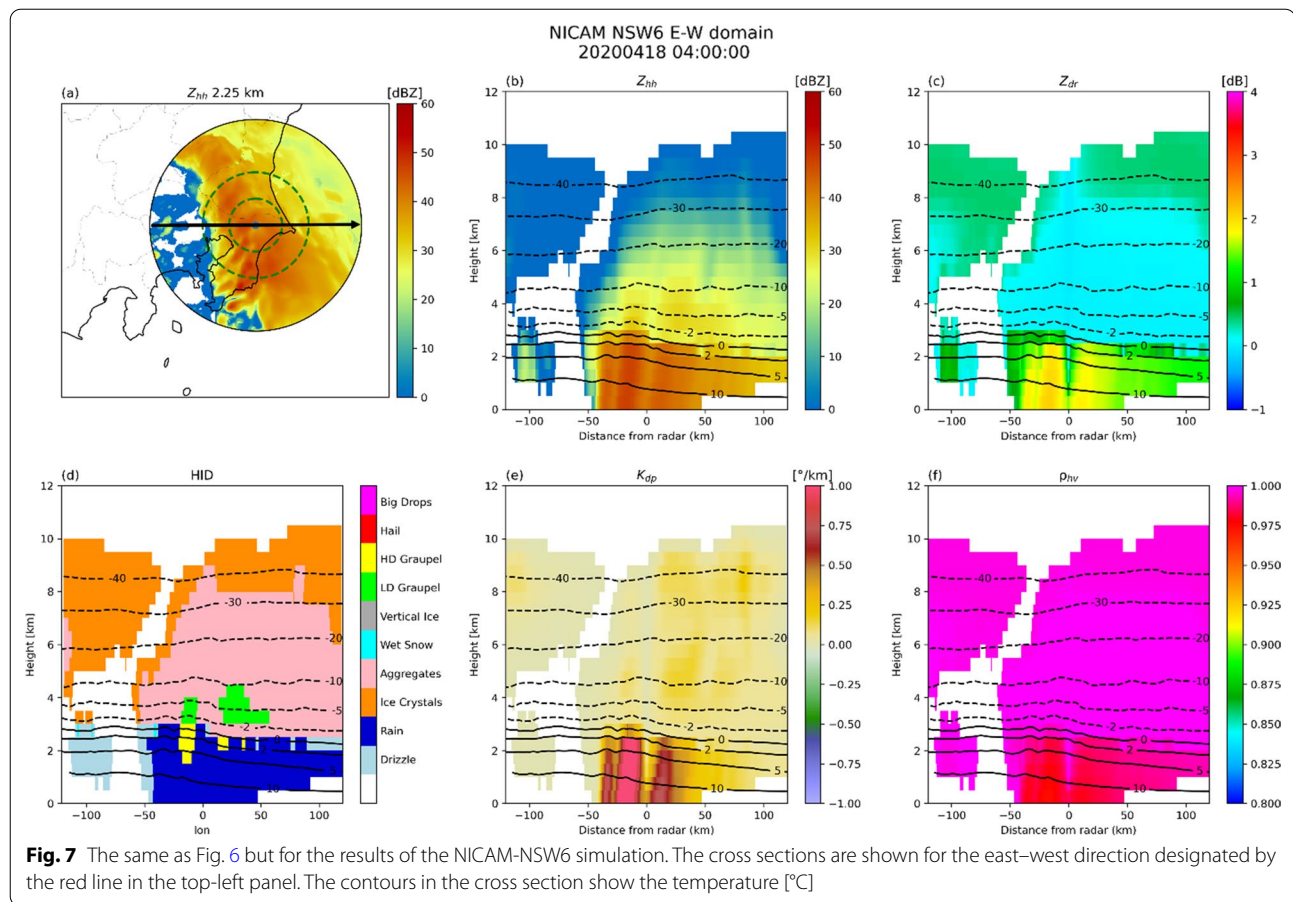


Fig. 6 Radar observation by the Narita radar at 04:00 UTC, April 18, 2020. Top row: **a** horizontal distribution of radar reflectivity [dBZ] (elevation angle 0.7°), vertical cross sections of **b** radar reflectivity Z_{hh} [dBZ] and **c** differential reflectivity Z_{dr} [dB]. Bottom row: vertical cross sections of **d** cloud types, **e** specific differential phase K_{dp} [°/km], and **f** copolar correlation coefficient ρ_{hv} . The vertical cross section is located along the straight line in the upper left figure (azimuth angle 239.5°)



band model. Thus, we must be careful about interpreting the results of the simulated signals, particularly for solid particles.

To visualize the dual-polarization Doppler weather radar data, we use Py-ART (The Python ARM Radar Toolkit) (Helmus and Collis 2016).

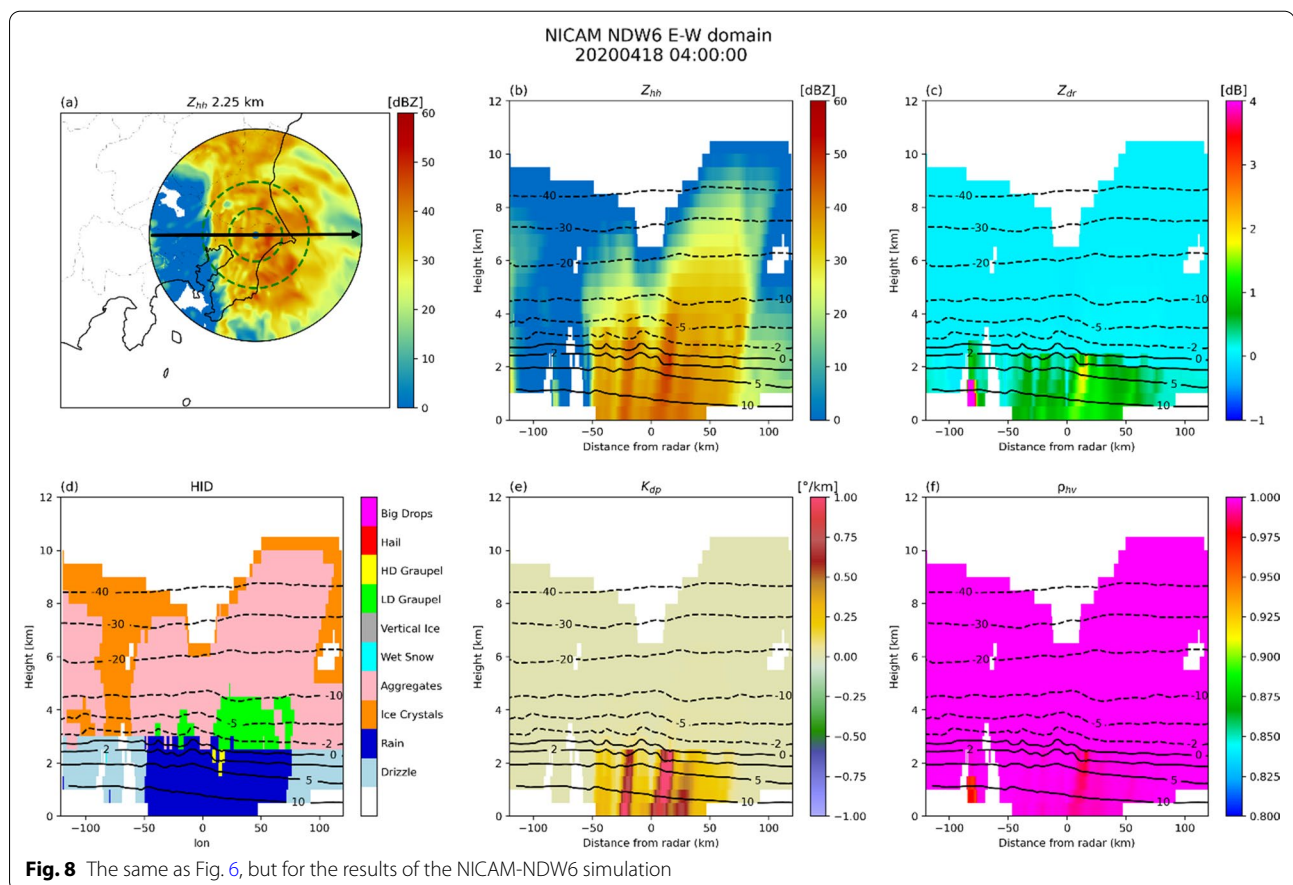
3 Results

3.1 Overview

We evaluate the cloud and precipitation characteristics of the models by comparing a case study of a weather event. In general, cloud and precipitation statistics are equilibrated on a daily scale (Matsui et al. 2015). We chose a case of a severe convective storm associated with an extratropical cyclone that passed over the Kanto region on April 18, 2020. We assume that a single event captures representative statistics of clouds and precipitation and gives plenty of data for model evaluation. A bias found

in one case generally emerges in other cases because cloud microphysics depends primarily on thermodynamic conditions. However, other weather events may have different statistical properties. One may need to collectively conduct evaluations for various weather events to improve cloud microphysics schemes further. Further evaluation will be conducted in subsequent studies using the methodology proposed in this study.

Figure 3 shows a weather chart at 00:00 UTC on April 18, 2020. At this time, a synoptic-scale extratropical cyclone was developing around Japan, and the central area of the low-pressure system was approaching the Kanto region. Figure 4 shows the rainfall distribution at 04:00 and 06:00 UTC on April 18, 2020. Around this time, the mesoscale convective systems around the central area of the low-pressure system were active in the Kanto region, and quasi-linear rainfall distribution from the north-northeast (NNE) to the south-southwest (SSW)



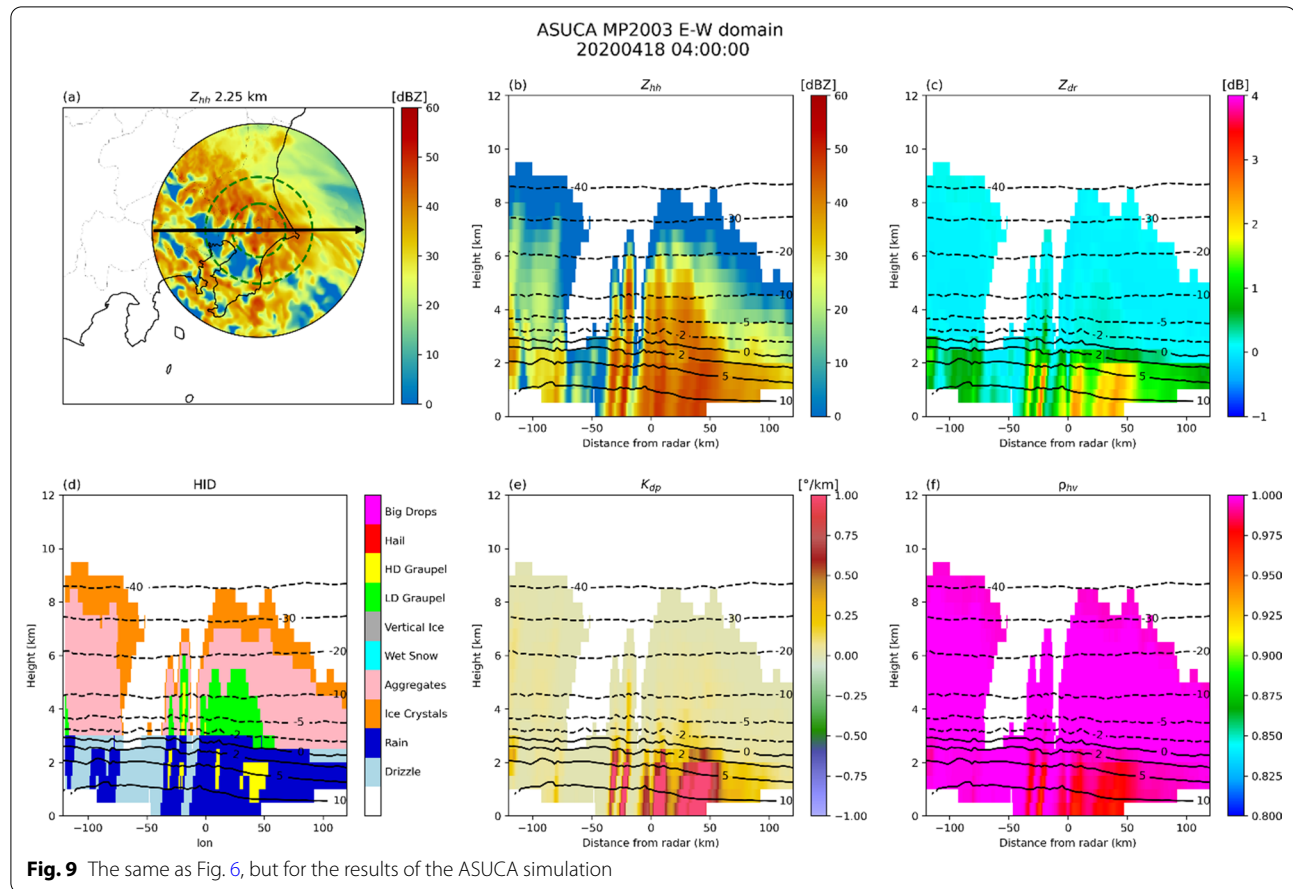
formed a frontal structure (06:00 UTC). Figure 4 compares the results of numerical simulations by NICAM, ASUCA, and SCALE with the observation. The initial value for all the simulations is set at 00:00 UTC on April 18. Each simulation reproduces the overall convective system embedded in the central area of the low-pressure system over the Kanto region but at a relatively coarser resolution than the observation. The observed finer-scale rainband system is broken into several rain areas in the simulations. This result suggests that higher resolution is required to reproduce such a linear rainband system realistically.

Figure 5 (right) shows the time sequence of the 1-h accumulated rainfall amount averaged over the rectangular area shown in Fig. 5 (left), which also shows the horizontal view of the ranges of the two radars at Haneda and Narita. The observed rainfall amount is the Radar-rain gauge Analyzed Precipitation provided by the Japan Meteorological Agency. The simulations captured the overall evolution of 1-h rainfall amount between

00:00–01:00 and 11:00–12:00 UTC on April 18. This comparison indicates that all the models capture convective systems embedded in the extratropical cyclone, though the detailed structure of mesoscale convective systems differs from the observation. For the present purpose of evaluating cloud and precipitation characteristics, we use these datasets as they represent typical convective systems in the simulations.

3.2 Cross sections

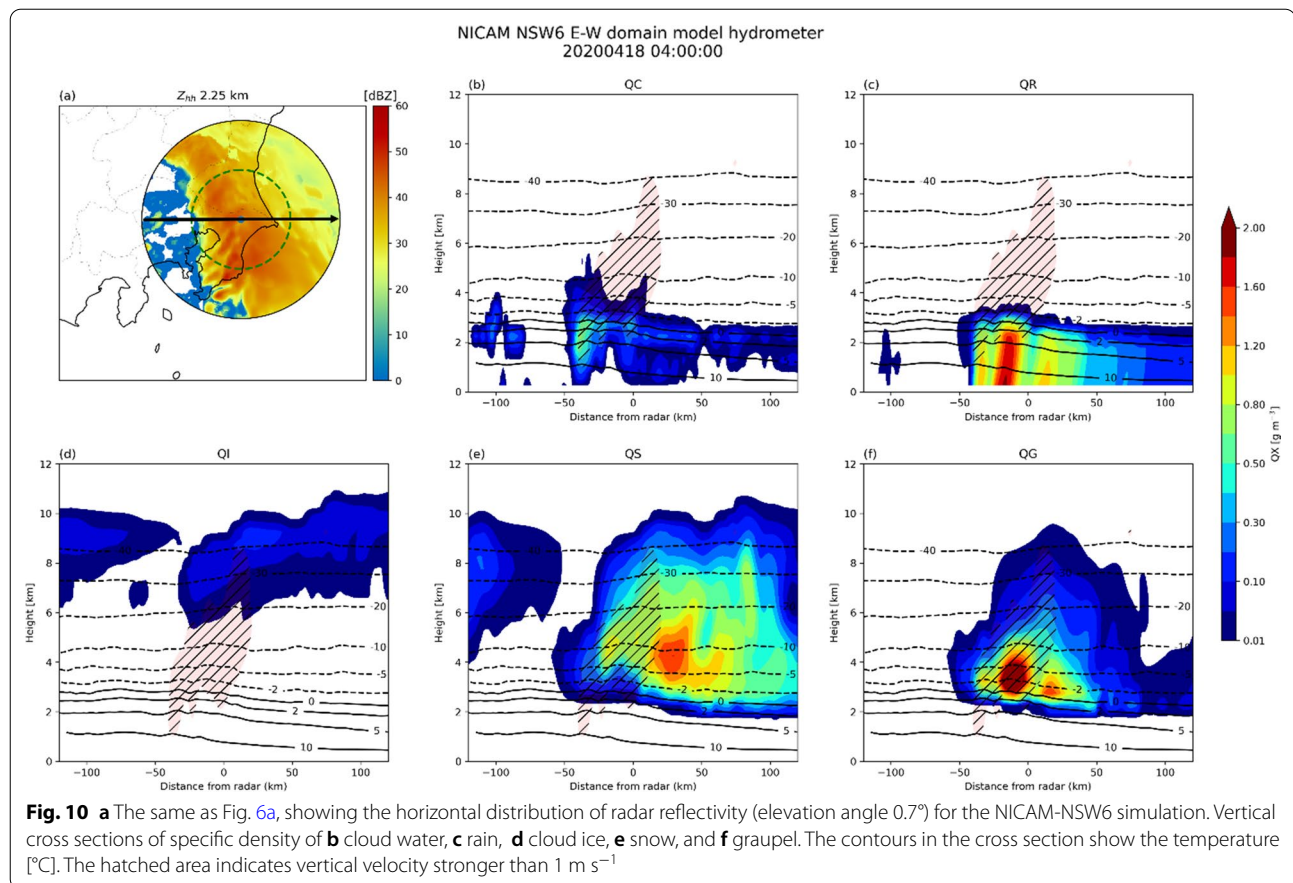
Figure 6 shows the horizontal distribution and vertical cross section of the radar parameters at the Narita radar just before 04:00 UTC. Precipitation spread over the southern Kanto region in the vertical cross section obtained in Range–Height Indicator (RHI) mode. The cross section of radar reflectivity Z_{hh} shows that the intensity is more prominent in the lower layers and decreases rapidly above an altitude of 3 km. This contrast is because liquid water with a strong reflectivity spreads



below an altitude of 3 km, and the solid phase prevails above 3 km. A melting layer exists between these layers, showing an increase in radar reflectivity around an altitude of 3 km. The melting layer is visible in the polarization parameters: i.e., differential reflectivity Z_{dr} , specific differential phase K_{dp} , and copolar correlation coefficient ρ_{hv} . There is a significant decrease in ρ_{hv} , and Z_{dr} shows various positive and negative values. This signal of the melting layer is due to the presence of water substances in the mixed phases around the melting layer, including water, ice with complex shapes, and ice covered by melting water. In Hydrometeor Identification (HID) (Fig. 6d), Wet Snow and HD/LD Graupel are found near the melting layer, indicating that ice particles and rain in various phases are mixed. Focusing on the rain in the lower layer, Z_{dr} and K_{dp} tend to be large where the reflection intensity is high (e.g., at around $x = -80$ km). These larger values of Z_{dr} and K_{dp} indicate that larger hydrometeor particles

exist in the case of strong precipitation. However, the contrasts in Z_{dr} and K_{dp} do not correspond exactly, indicating the difference in the particle shape distribution. In general, Z_{dr} is more sensitive to larger particles and can be noisier for moderate size particles.

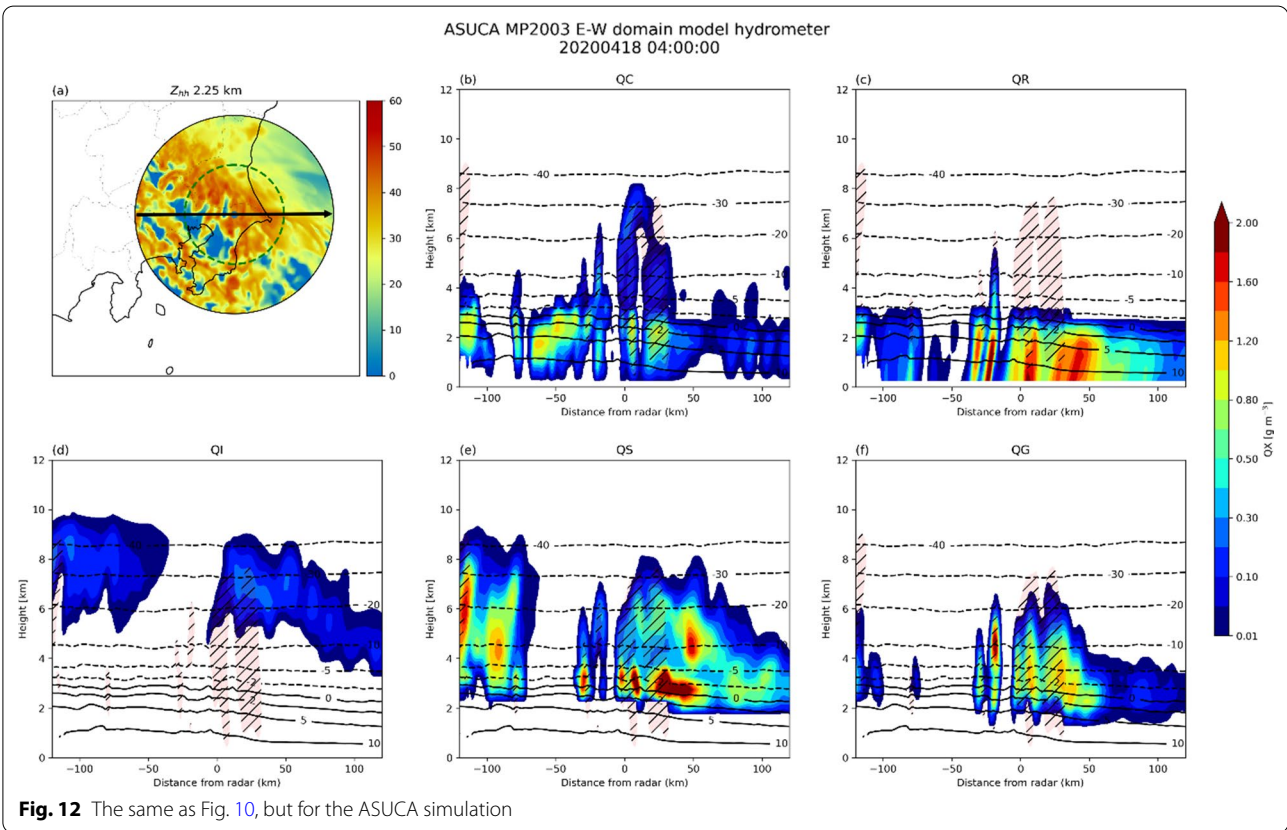
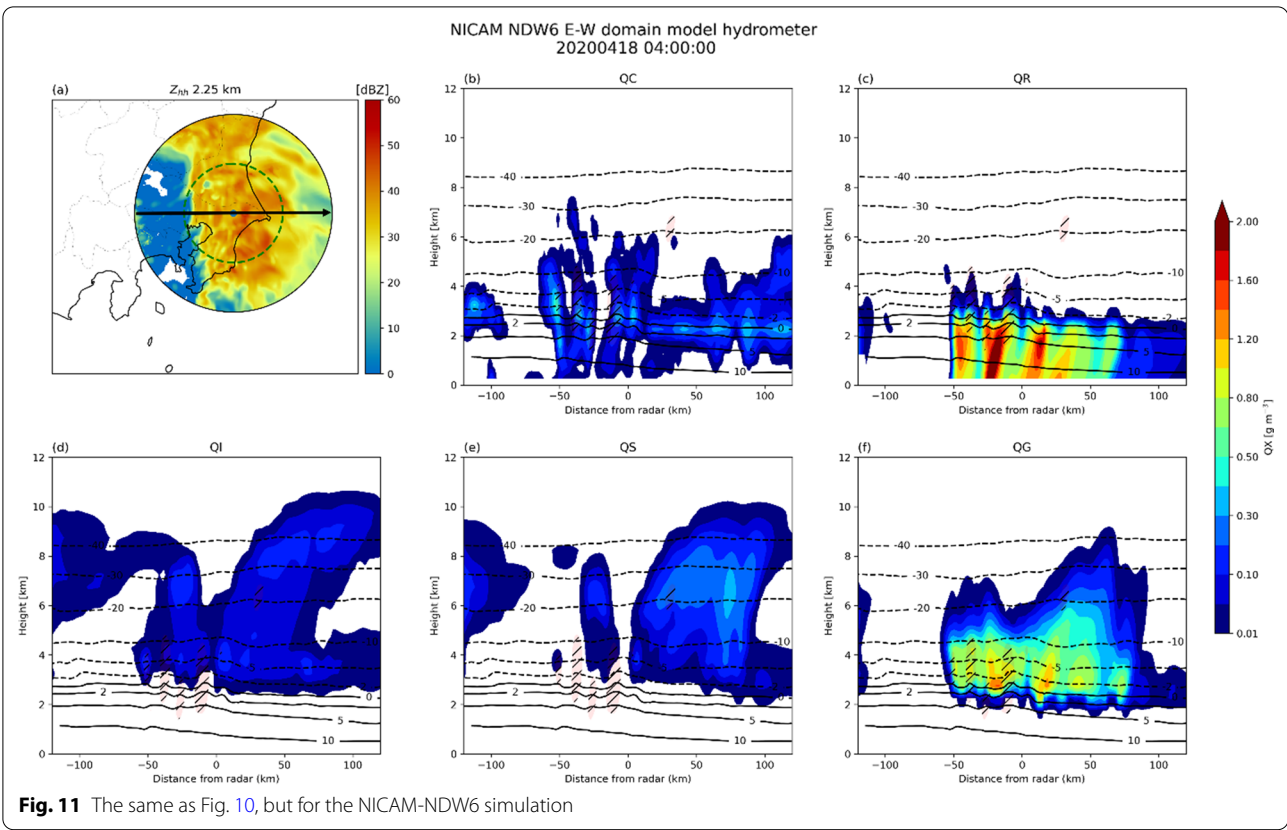
Figures 7, 8 and 9 show the corresponding simulated polarimetric radar signals using J-Sim with POLAR-RIS; Figs. 7 and 8 are for the NICAM simulations with the two cloud microphysics schemes NSW6 and NDW6, respectively, and Fig. 9 is for the ASUCA simulation. The vertical cross sections are shown in the zonal direction indicated by the black arrow in Figs. 7a, 8a and 9a, and temperatures are indicated by solid and dotted curves. Qualitatively, the vertical distribution of the radar reflectivity Z_{hh} is well reproduced, although the cloud area west of Narita is relatively small in all the simulations. Z_{hh} in NICAM-NDW6 in the rain layers below about 3 km is weaker than NICAM-NSW6 and is closer to the

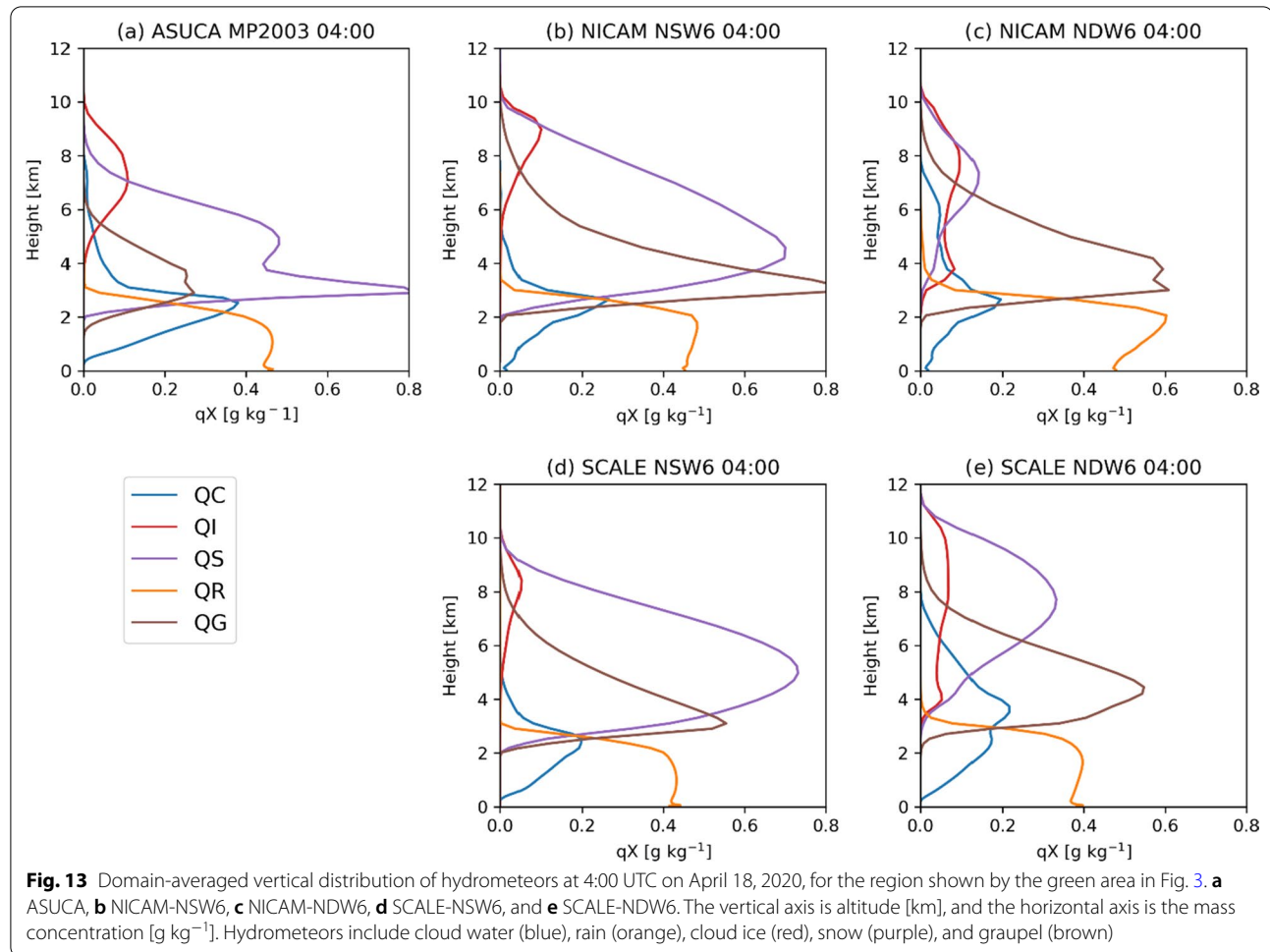


observation (Figs. 6b, 7b, 8b). The melting level signals are not simulated in Figs. 7, 8 and 9 because polarization parameters cannot be calculated for melting particles in POLARRIS-f. The contrast in Z_{dr} and K_{dp} in the rain layers of all the simulations is much larger than in the observations (Figs. 6c, e; 7c, e; 8c, e; 9c, e). HID shows that the vertical extent of the graupel categories (HD/LD Graupel) is simulated differently above the melting level (Figs. 6d, 7d, 8d, 9d). Rain and Drizzle are simulated for rain below the melting level (lower than an altitude of 3 km), while only Rain is identified in the observation.

To understand the difference in the simulated polarimetric radar signals, we compared the distributions of each hydrometeor category for the three simulations in Figs. 10, 11 and 12, showing the vertical cross sections of mass concentrations of cloud water, rain, cloud ice, snow, and graupel along the zonal direction shown by the red line in the horizontal view (Figs. 10a, 11a, 12a). For the synthesis view, Fig. 13 shows the vertical distribution of

mass concentrations of these five hydrometeor classes averaged over the domain (Fig. 5, green square) by comparing all the simulation results. The vertical cross section and the vertical distribution of mass concentration of rain are not so different between NICAM-NSW6 and NICAM-NDW6 (Figs. 10c, 11c; Fig. 13), while the radar reflectivity Z_{hh} is larger in NICAM-NSW6 than in NICAM-NDW6 (Figs. 7c, 8c), suggesting that raindrop size in strong rainfall areas is larger in NICAM-NSW6 than in NICAM-NDW6. Cloud water in ASUCA extends to the upper level at around 8 km in the convective areas (Fig. 12b), similar to NICAM-NDW6. For the ice phase, the vertical distributions of snow and graupel are very different among all the simulations (Figs. 10d–f, 11d–f, 12d–f; Fig. 13); mass concentrations of snow and graupel are larger in NICAM-NSW6 than in NICAM-NDW6 (Figs. 10e, f; 11e, f). Cloud ice spreads above the melting level in NICAM-NDW6, while it is confined to the upper layers above 7 km in NICAM-NSW6. Figure 12



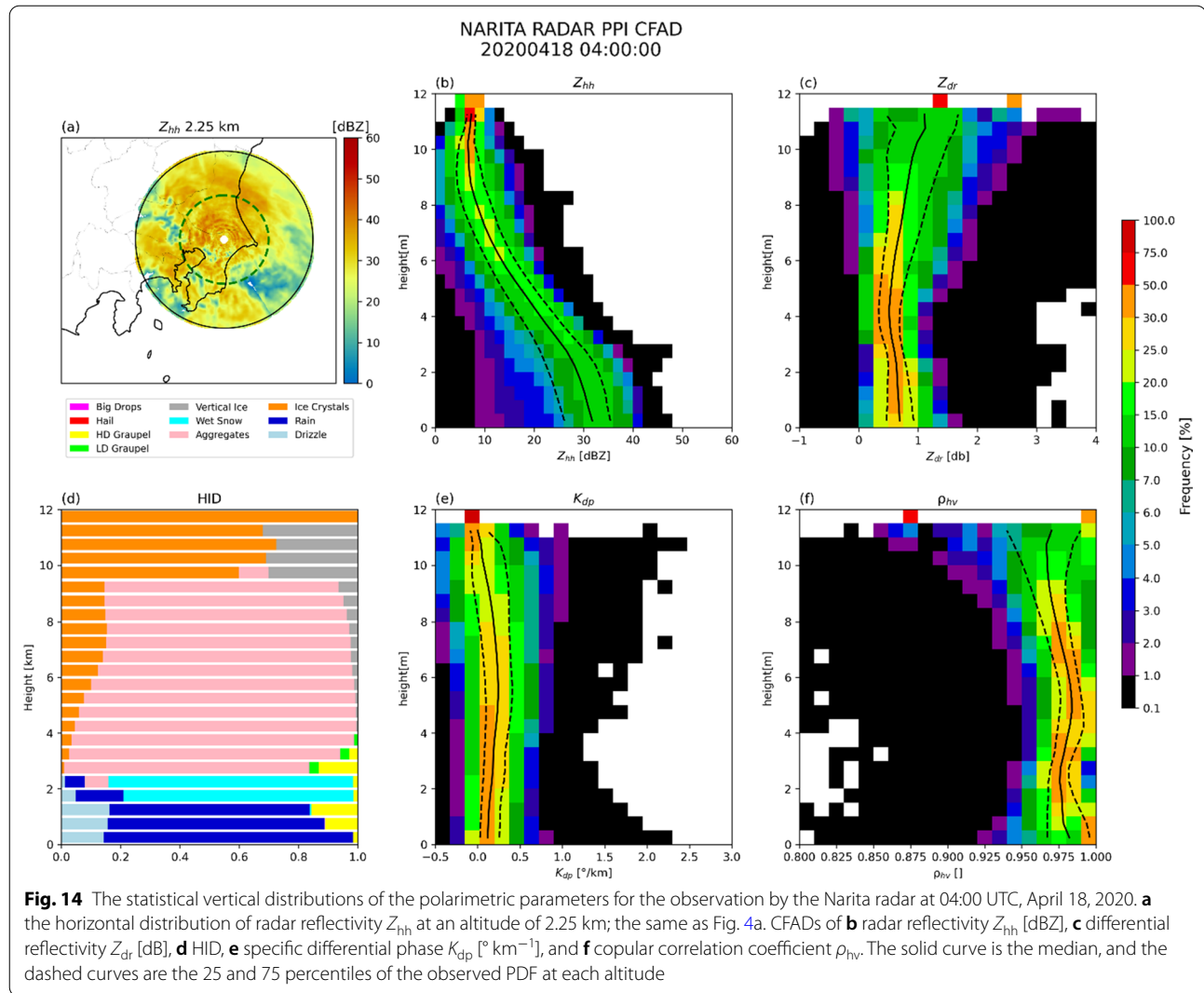


shows that cloud ice in ASUCA also exists in the upper layers, while snow and graupel prevail lower than cloud ice (Fig. 12d–f). Figures 10, 11 and 12 also indicate areas of the vertical velocity stronger than 1 m s^{-1} (hatched); they show that all hydrometeor categories become more abundant in regions of stronger upward motion.

A comparison of all the models in Fig. 13 shows the diversity in simulating the ice categories of cloud ice, snow, and graupel; the vertical distribution of these hydrometeors strongly depends on the model. Notable differences are seen in the height of the peak of snow mass concentration and the relative magnitudes of the peak values between snow and graupel. Cloud ice prevails down to the melting level of around 3 km for the two models with NDW6, while it exists only above 5 km for the models with single-moment schemes. Mass concentrations of rain are much closer between the models;

ASUCA shows a larger mass concentration of rain and more vertical distributions above the melting layer up to 4 km (Fig. 13a).

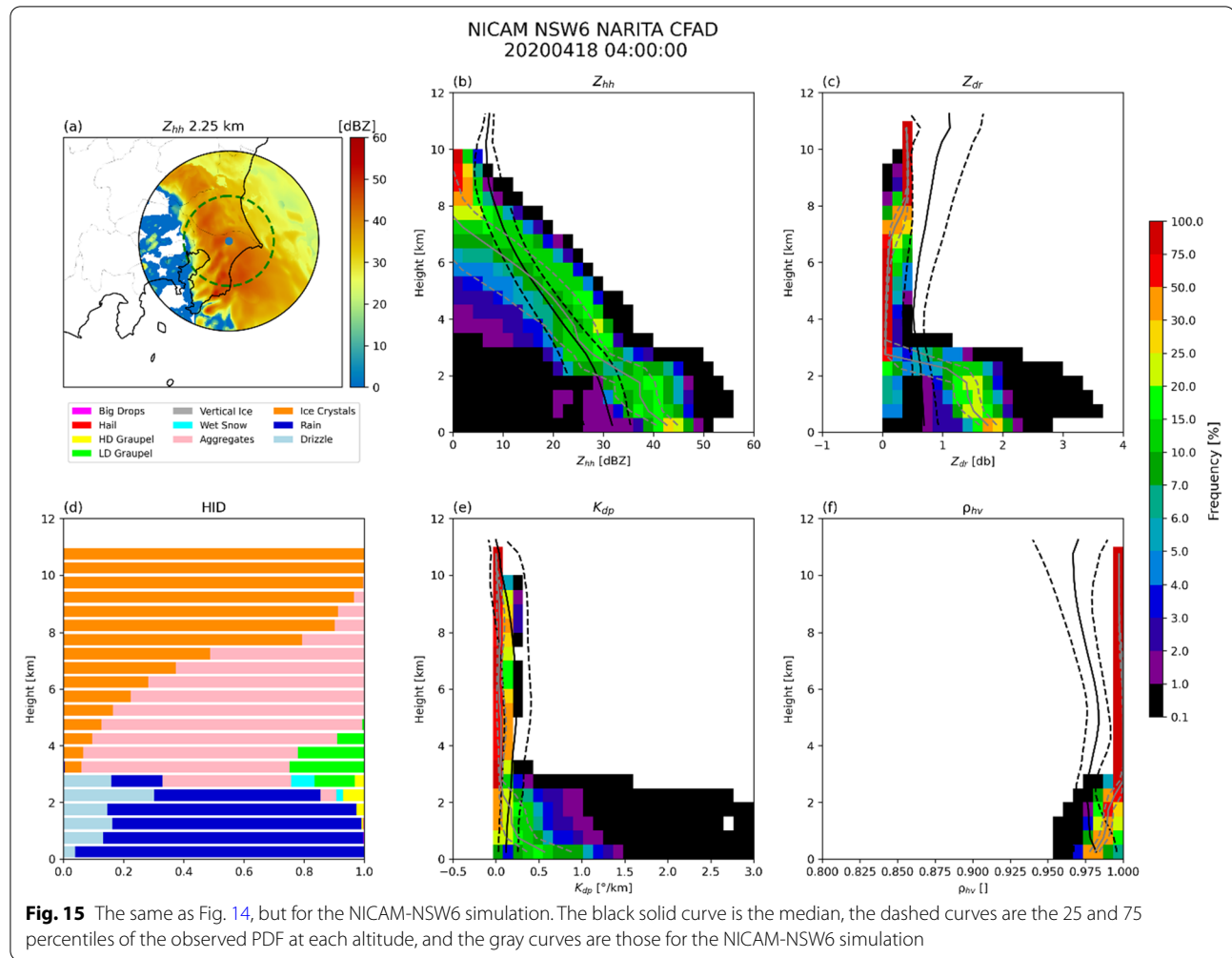
Figure 13 shows that the difference between NSW6 and NDW6 is similar between NICAM and SCALE. The altitude of maximum mass concentration of snow is higher for NDW6 than for NSW6, and the relative magnitudes of the peak values of snow versus graupel are smaller for NDW6 than for NSW6. The altitudes where cloud ice and cloud water prevail are deeper for NDW6 than for NSW6; cloud ice exists above an altitude of 3 km for NDW6 compared to above 5 km for NSW6, while cloud water reaches up to 8 km for NDW6 compared to 6 km for NSW6. That is, in NDW6, there are altitudes where cloud ice and cloud water coexist between 3 and 8 km, while there are few overlapping



altitudes of the two categories in NSW6. In more detail, we can see the differences between NICAM and SCALE in Fig. 13, even for the same cloud microphysics scheme. Among the differences, the height and the value of the maximum mass concentration of snow are visible. These differences suggest that other factors (e.g., the dynamical cores, resolutions, or initial conditions) affect the distributions of hydrometeors. By conducting other case studies, we will reveal the robustness of the difference between NICAM and SCALE. Hereafter, we mainly analyze the results for NICAM and ASUCA, and details of the results for SCALE are summarized in “Appendix 2.”

3.3 Contoured frequency diagrams

Figures 14, 15, 16 and 17 compare the contoured frequency by altitude diagrams (CFADs) of the polarimetric radar signals and cloud types, statistically analyzed in the green domain shown in Fig. 5 for the observation and the three simulations. These CFADs can be used for quantitative and statistical evaluation of cloud microphysics. For NICAM-NSW6 (Fig. 15), Z_{hh} in the lower layer is stronger than in the observation (Fig. 14), and the maximum of Z_{hh} decreases rapidly around the melting layer and closer to the observation. Between altitudes of 0 and 2 km, Z_{dr} has a probability peak between 1.5 and 2 dB and is larger than the observation. For NICAM-NDW6 (Fig. 16), Z_{hh} is consistent with the observation between



the altitudes of 0 and 2 km, but it is stronger above the melting layer than in the observation. The magnitude of Z_{dr} near the surface between the altitudes 0 and 1 km is consistent with the observation. For ASUCA (Fig. 17), as in NICAM-NSW6, Z_{hh} in the lower layer is overestimated compared to the observation. For all the simulations, ρ_{hv} has smaller variability than the observation in the lower layer below the melting layer and is close to 1 above the melting level due to the smaller dispersion of habits of ice particles in the simulations. In the lower layer, the size of rain particles affects the variability of ρ_{hv} ; NICAM-NDW6 shows ρ_{hv} is closer to the observation, while NICAM-NSW6 and ASUCA represent smaller values of ρ_{hv} near the surface because the size is directly related to the mass concentrations of rain.

In the lower layers below an altitude of 2 km, the two polarimetric parameters Z_{dr} and K_{dp} in NICAM-NSW6 are generally larger than the observations. In contrast,

these parameters in NICAM-NDW6 are closer to the observations.

Ice particles dominate the layer above the melting level (3–4 km). Because the shapes of ice particles affect polarimetric parameters, it is generally difficult to evaluate numerical model results in which the shapes of ice particles are not considered. In general, however, radar reflectivity Z_{hh} can be used to evaluate ice particles because it reflects the size of ice particles. In the layer just above the melting level (3–4 km), the maximum value of Z_{hh} in NICAM-NSW6 is smaller than the observation. In contrast, the maximum values of Z_{hh} in NICAM-NDW6 and ASUCA are larger than the observation. The polarimetric parameters, Z_{dr} , K_{dp} , and ρ_{hv} , all show a small spread above the melting level; Z_{dr} and K_{dp} are close to zero, and ρ_{hv} is almost 1. These small spreads are due to the assumptions on ice particles used for POLARRIS (Matsui et al. 2019b), which might inhibit a larger spread of these radar parameters.

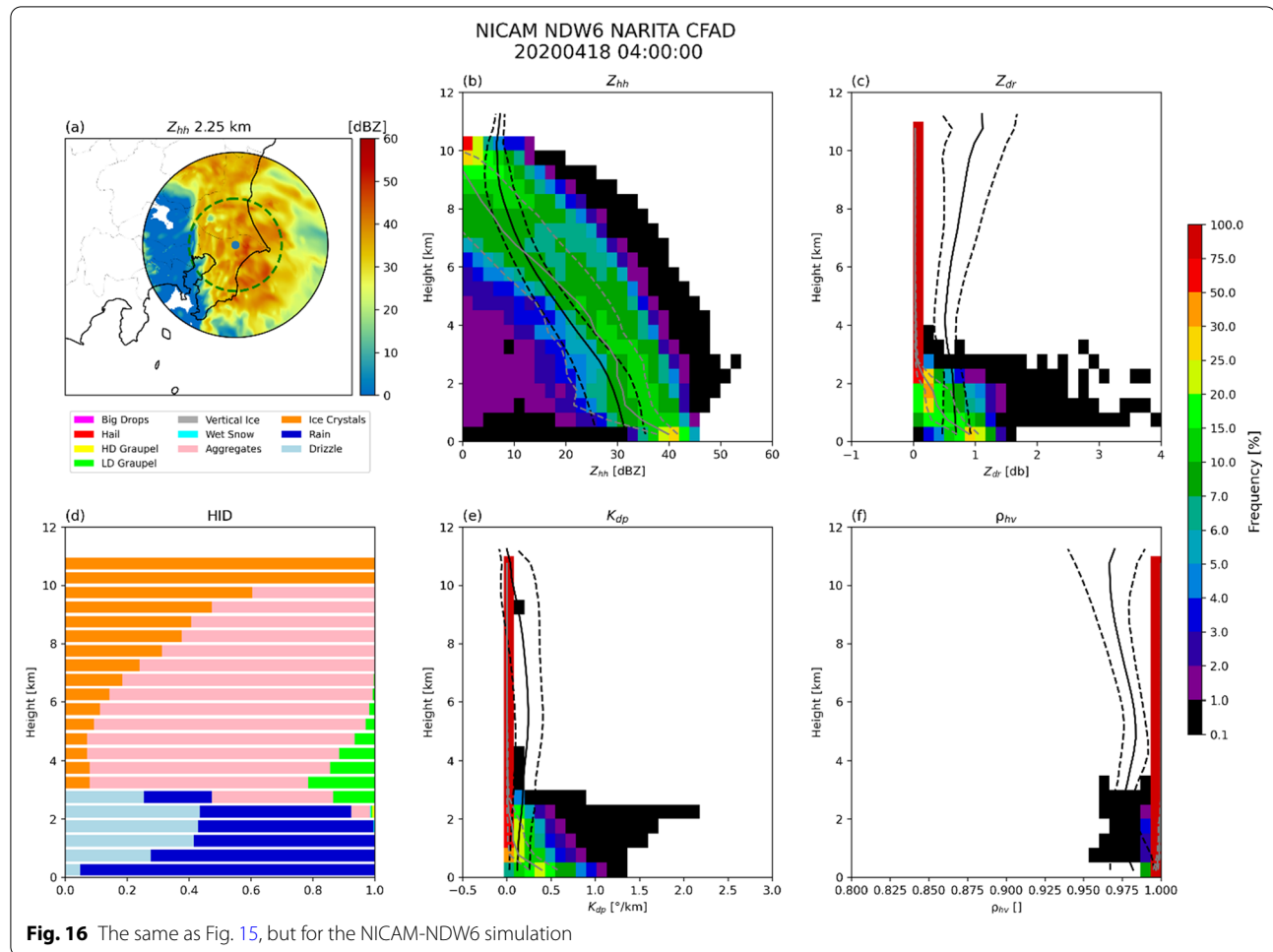


Fig. 16 The same as Fig. 15, but for the NICAM-NDW6 simulation

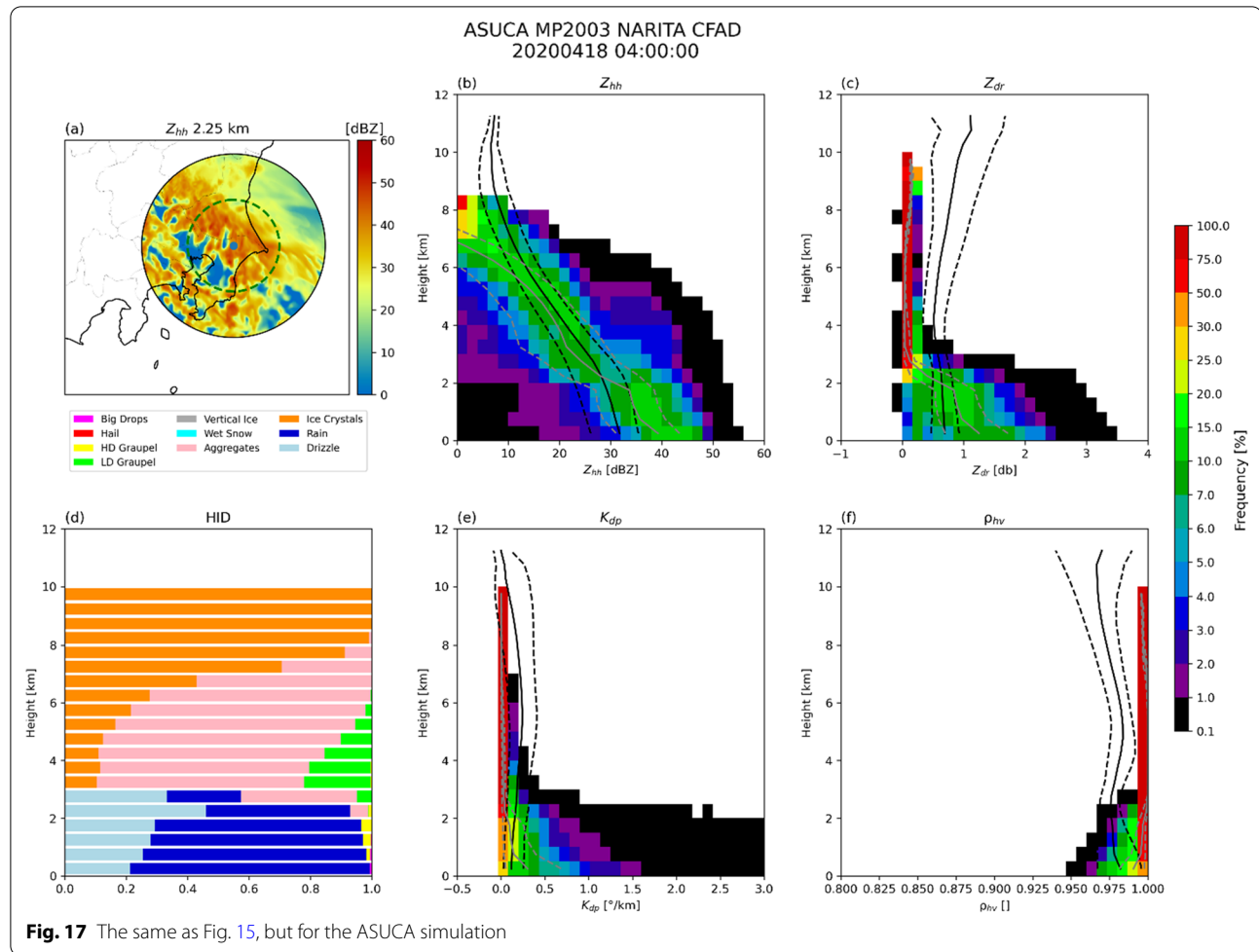
3.4 Hydrometeor Identification

We now compare the distributions of cloud particle categories using HID between the observation and the models. The overall differences can be viewed in the CFAD of HID in Figs. 14d, 15d, 16d and 17d. We should note that the HID of the simulations does not correspond to the hydrometeors of the cloud microphysics schemes used in the numerical models. HID is derived solely from the polarimetric parameters, and the characteristics of HID distribution must be viewed with these parameters. HID diagnosed for the observed signals is also affected by the uncertainties of the observation, such as the precipitation attenuation and other noises. We compare the HID of the observation with that of the three simulations in the layers below, near, and above the melting level, located around an altitude of 3–4 km.

The observation shows a mixture of Rain, Drizzle, and HD Graupel for the layer below the melting level (Fig. 14d). For NICAM-NSW6 (Fig. 15d), the frequency of Drizzle is similar to the observation. For

NICAM-NDW6 and ASUCA (Figs. 16d, 17d), Drizzle is more often diagnosed than the observed HID. This suggests that the size of the rain categories in NICAM-NSW6 is larger than in NICAM-NDW6 and ASUCA. As for HD Graupel, all the simulations show a smaller frequency than the observation; this might be a bias in the simulations.

Near the melting level (3–4 km), Wet Snow is most frequent around an altitude of 2 km and HD Graupel is observed above and below the melting level (Fig. 14d). HD Graupel is mixed with Wet Snow just around the melting level (Fig. 6d; $x \sim 50$ –100 km), which indicates that HD Graupel and Wet Snow coexist in the precipitating regions of the ice phase particles near the melting level. Wet Snow is not diagnosed in all the simulations. Above the melting level up to an altitude of around 5–6 km, LD Graupel is diagnosed in the simulations instead of HD Graupel. This result implies that the comparison with the observation detects a bias in



the size of graupel in the numerical models. This aspect will be discussed in the next section.

Above the melting level (3–4 km), HID is barely reliable up to an altitude of about 10 km because of the limitation of the assumptions of HID (Matsui et al. 2020). In the observation, Aggregates, Ice Crystals, and Vertical Ice exist at altitudes of 4–10 km, with Aggregates being the most frequent occurrence (Fig. 14d). Only Ice Crystals and Aggregates exist in all three simulations without Vertical Ice (Figs. 15d, 16d, 17d). The cloud microphysics schemes that were used do not include assumptions of the shape of ice particles, so we speculate that these HIDs of ice particles are based solely on particle size. The probability of Ice Crystals is larger than the observation for all the simulations. This difference between the observation and the simulations is related to the difference in the probability of Z_{hh} at these altitudes (Figs. 14b, 15b, 16b, 17b); near an altitude of 8 km, the highest probability of Z_{hh} is observed at larger values of Z_{hh} compared to those

of the simulations: about 10 dBZ in the observation (Fig. 14b) vs. < 5 dBZ in NICAM-NSW6 and ASUCA (Figs. 15b, 17b). For NICAM-NDW6 (Fig. 16d), the probability of Ice Crystals is the closest to the observation. However, the radar reflectivity at the higher level is affected by the attenuation and other noises, and smaller signals are not always captured accurately, as inferred from Fig. 6b.

The two hydrometeor categories of Rain and Drizzle are classified in the lower layer. Although we do not distinguish between rain and drizzle in the cloud microphysics schemes, the simulated radar signals distinguish these two cloud types. The size distribution of rain particles is used in CSU hydrometeor classification. The difference in HID between Rain and Drizzle suggests inconsistency in the particle size of the rain categories used in the simulations. It will also be necessary to investigate how the parameters related to non-sphericity, which is not explicitly defined in the cloud microphysics scheme, can be included in J-Sim/

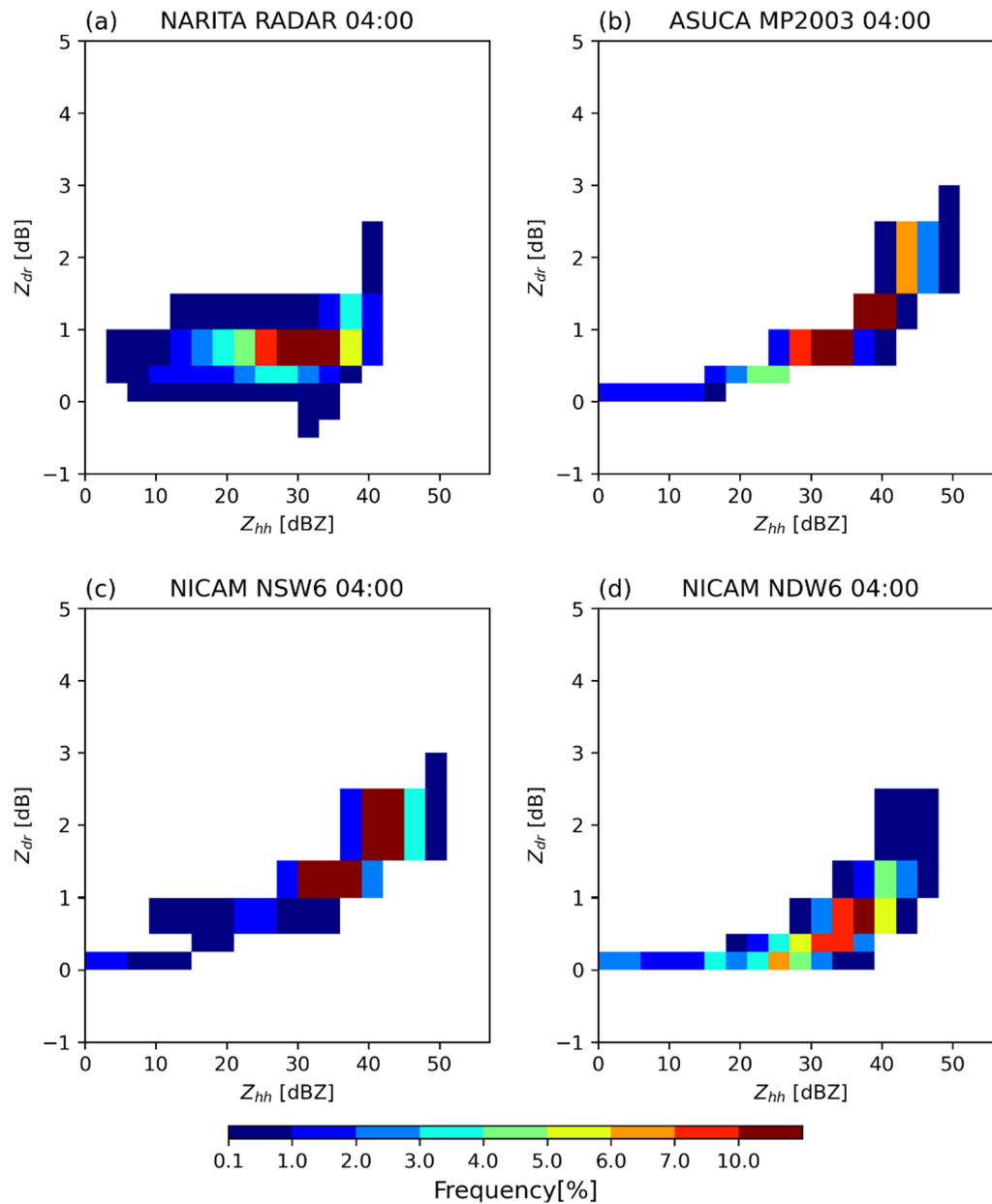


Fig. 18 Joint probability distributions between Z_{hh} [dBZ] and Z_{dr} [dB] at an altitude of 1.75 km at 04:00 UTC, April 18, 2020. **a** The Narita radar; **b** ASUCA; **c** NICAM-NSW6; and **d** NICAM-NDW6

POLARRIS. We note from the above results that Rain is detected up to 2 km, which is higher than the observation in which Wet Snow is diagnosed. In addition, the vertical extent of simulated probability of HD/LD Graupel is deeper than the observation, extending to altitudes 4–6 km above the melting level. In contrast, the observation shows that they are categorized as HD Graupel and are confined below an altitude of 4 km.

4 Discussion

By comparing the observation and the simulations, we found that the polarimetric parameters are useful for identifying the model bias of the rain processes in the lower layer below the melting level (around an altitude of about 3 km). In contrast, for the ice particles above the melting level, the cloud microphysics assumptions of the numerical models used in this study do not fully

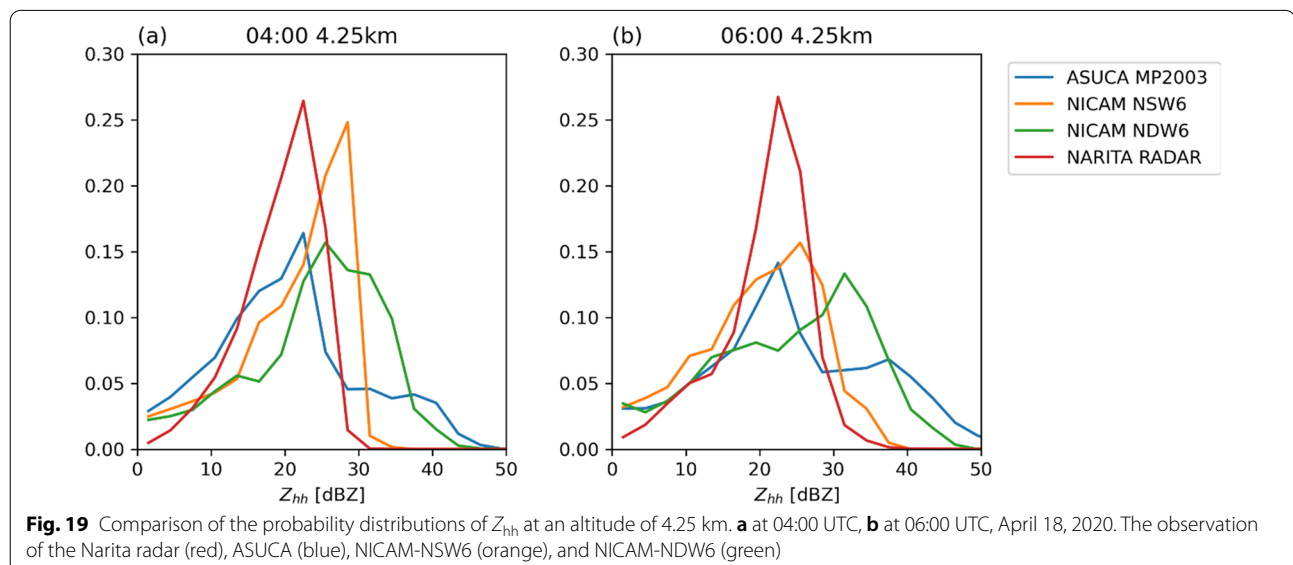
reproduce realistic polarimetric parameters comparable with the observations. In particular, we do not take account of the shapes of hydrometeors for the cloud ice, snow, and graupel categories in the models. The shapes and the spatial orientation of the different hydrometeors are assumed in the observation simulators (Matsui et al. 2019a, b). That is why the polarimetric parameters have smaller dispersions, such that Z_{dr} and K_{dp} are close to zero, and ρ_{hv} is close to 1 above the melting level for all the simulations (Figs. 15, 16, 17). Thus, with the current complexity of the cloud microphysics assumptions, the polarimetric parameters do not help detect the bias of the models. This limitation was pointed out by Matsui et al. (2020). For Z_{hh} , however, the difference among the models and between the models and the observation can be identified because Z_{hh} reflects the particle size. In particular, the maximum values of Z_{hh} in the layer just above the melting level are different between the observation and the models (Figs. 14b, 15b, 16b, 17b), which we think comes from the assumption of the size distribution in the graupel category in the model. Here, we summarize the comparisons of the following two aspects: Z_{hh} and Z_{dr} at an altitude of 1.75 km, which is in the lower layer below the melting level for validation of rain particles, and Z_{hh} at the altitude of 4 km, which is just above the melting level, for validation of graupel particles.

Figure 18 shows the joint probability distributions between Z_{hh} and Z_{dr} at an altitude of 1.75 km. For the simulations using the single-moment bulk schemes (NICAM-NSW6, ASUCA), Z_{dr} is uniquely related to Z_{hh} . Both results show overestimations of Z_{dr} : Fig. 14 (observation) vs. Figs. 15 and 17 (NICAM-NSW6, ASUCA). That is, NICAM-NSW6 and ASUCA

overestimate the particle size of rain. The simulation with the double-momentum scheme, NICAM-NDW6, shows a closer resemblance of the probability to the observation (Figs. 14 and 16). A similar analysis to Fig. 18 was presented by Putnam et al. (2017) and Bringi et al. (2020) and is used for evaluating the size sorting of hydrometeors, including rain.

The snow and graupel simulations just above the melting level between altitudes of 4 and 6 km differ from the observation. Figure 19 compares the probability of Z_{hh} at an altitude of 4 km at two snapshots, 04:00 and 06:00 UTC. The observation and NICAM-NSW6 show a clear cut-off of Z_{hh} around 30 dBZ, indicating the limitation of the maximum size of ice particles. Both NICAM-NDW6 and ASUCA show larger probabilities between 30 and 40 dBZ, and much larger ice particles exist at about 50 dBZ. The similarity between the observation and NICAM-NSW6 is specifically noted because the assumption for the graupel category in NICAM-NSW6 is based on Roh and Sato (2014), in which the tropical condition is assumed.

The comparison between the observation and the simulations can be summarized as follows. The simulation with the double-moment scheme, NICAM-NDW6, reproduced the comparable polarimetric radar characteristics as the observation in the Z_{hh} - Z_{dr} space. However, the simulations with the single-moment schemes, NICAM-NSW6 and ASUCA, show larger raindrop sizes in stronger rain areas compared to the observation. Because Z_{hh} uniquely determines Z_{dr} in the single-moment schemes, the stronger precipitation is associated with the larger raindrop size, unlike the observation. For the larger ice particles just above the melting level around 4 km, NICAM-NDW6 and ASUCA produced



larger particles of graupel or snow, while NICAM-NSW6 has a similar cutoff of the high values of Z_{hh} as in the observation.

5 Conclusions

This paper introduces ULTIMATE, a framework for collaborative research between observation and numerical modeling using various observation data in the Kanto region. An example of validating numerical models using dual-polarization Doppler weather radars in the Kanto region is presented. ULTIMATE is intended to validate not only ordinary regional models but also global storm-resolving models (GSRMs) that can seamlessly be used as local and global models with common dynamical core and physics schemes.

We use multiple models for comparison: NICAM, SCALE, and ASUCA. Two cloud microphysics schemes, NSW6 and NDW6, are used for NICAM and SCALE. We propose utilizing the observation simulator of a dual-polarization Doppler weather radar, called POLARRIS, which is implemented in the Joint Simulator for Satellite Sensors (J-Sim). The vertical cross sections of the observed polarimetric radar parameters in the Range-Height Indicator (RHI) mode are compared with the simulated counterparts. The contoured frequency by altitude diagrams (CFADs) are used for quantitative and statistical comparisons between the observation and the simulations. The multiple model approach revealed the common bias of the polarimetric parameters in the single-moment scheme and the advantages of the two-moment scheme. Comparison between NICAM and SCALE, which use the same cloud microphysics schemes, shows similar overall results, although many factors other than cloud microphysics are different. This result indicates that the present assessment may be applicable as representative even if a single meteorological event is used.

Among various aspects of the comparisons, we pointed out the difference in the rain layer below the melting level (Fig. 18) and the characteristics associated with larger ice particles just above the melting layer (Fig. 19). The simulation with the double-moment scheme, NICAM-NDW6, reproduced the comparable polarimetric radar characteristics as the observation. However, the simulations with the single-moment schemes, NICAM-NSW6 and ASUCA, show relatively large raindrop sizes in stronger rain areas compared to the observation. For the larger ice particles just above the melting level around 4 km, NICAM-NDW6 and ASUCA produced larger particles of graupel or snow, while NICAM-NSW6 has a similar size of the ice particles to the observation. This result should be remarked on because NSW6 was

improved by comparing the TRMM observation in tropical regions (Roh and Sato 2014) and evaluated over the global scale (Roh et al. 2017). NICAM-NDW6 has also been developed mainly by comparing satellite observation over the global area (Sato et al., 2018).

In addition to the above point, the unique aspect of this study shows a path of the use of the local observation to a GSRM with a seamless approach. NICAM has been developed for a global model, and the global satellite observation data have been used to evaluate the current schemes NSW6 and NDW6 as described above. In the forthcoming studies, we will investigate cloud microphysics and other physical processes to improve polarimetric radar characteristics.

Under ULTIMATE, we will continue verifying and improving the cloud microphysics processes of numerical models using various ground-based observation data. The Kanto region, with about a $(100 \text{ km})^2$ square domain, is the target of a regional model with a horizontal mesh interval of about $O(\text{km})$. It can also be covered by higher-resolution models with a mesh interval of $O(100 \text{ m})$, called large-eddy simulations (LES), to resolve deep convective clouds (Ikuta et al. 2022). Roh et al. (personal communication) found that NICAM-NSW6 underestimates signals related to larger ice particles when observing intense deep convection in a tropical cyclone. Suppose we improve cloud microphysics schemes by validating numerical results in the Kanto region using NICAM simulations; in that case, the improved scheme can be readily tested in the global domain because NICAM can be used as both a global model and a regional model by utilizing a stretched grid.

Furthermore, by comparing and validating the global model with satellite observations, it will be possible to constrain the numerical model using satellite and ground observations. Based on such comparisons and verifications, it is possible to perform climate calculations using the improved global model. Using ground-based observations limited to the Kanto region, we can establish a path to use the global weather and climate simulation model; it may improve the accuracy of numerical weather prediction and reduce the uncertainty of climate prediction and climate sensitivity.

Appendix 1: Observation data for ULTIMATE

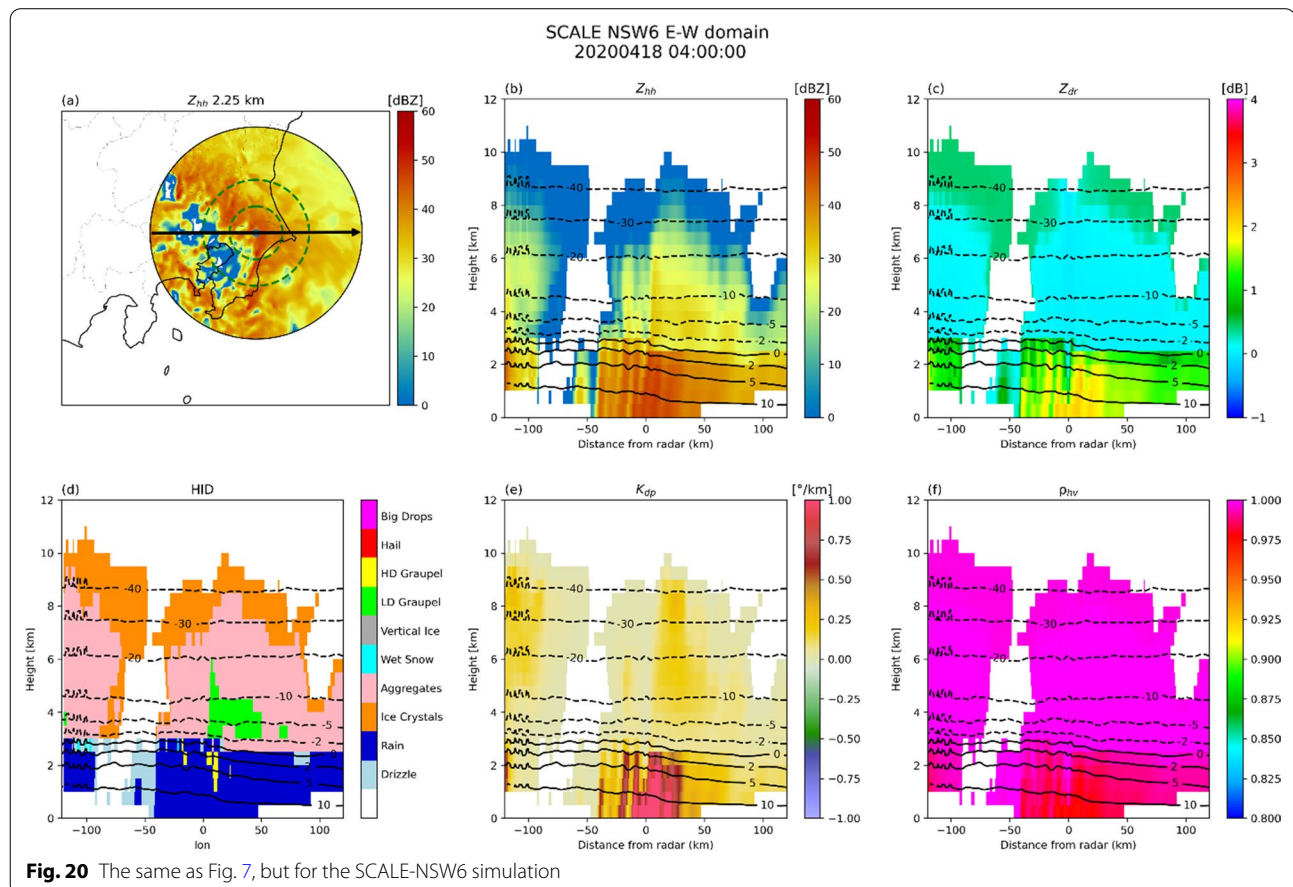
The observation data used for the ULTIMATE framework include the multi-frequency lidar (355 nm, 10 ch), the high spectrally resolved lidar (355 nm), high spectral resolution lidar (355 nm), Doppler lidar (355 nm), coherent Doppler lidar, HG-Spider 94 GHz Doppler radar,

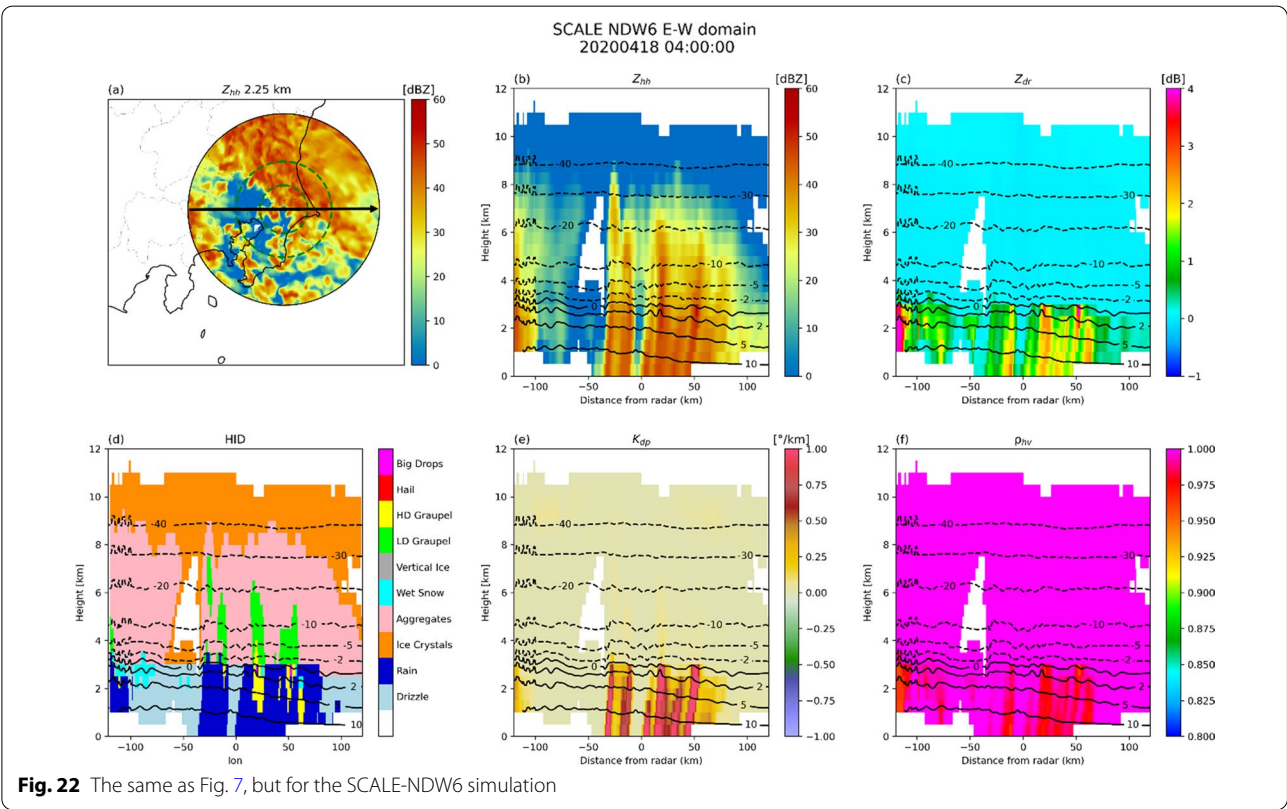
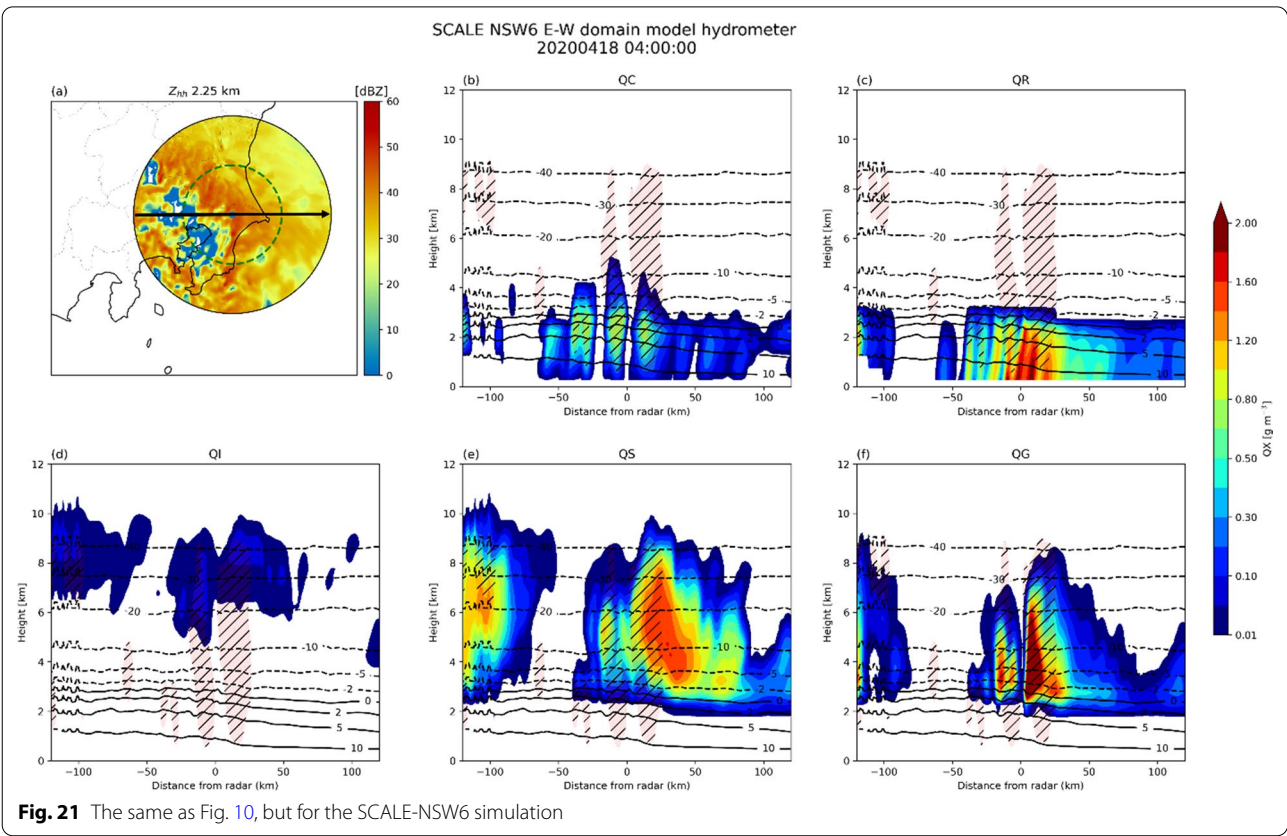
and wind profiler at NICT, and Mie polarization lidar (532 nm polarization, 1064 nm), multi-view angle multiple-scattering polarization lidar (532 nm), Multi-view Angle Multiple Scatter Polarization LIDAR (532 nm), and High Spectral Resolution LIDAR (532 nm). These are deployed by the EarthCARE satellite validation team of Kyushu University and the National Institute for Environmental Studies (NIES). The National Research Institute for Earth Science and Disaster Prevention (NIED) observes cloud and rain particle size distributions using the Fog Monitor and Laser Precipitation Monitor at Tokyo Sky Tree for ground validation. Existing X-band and Ka-Band radar data in NIED are available. In addition, routine observation data from JMA are available. In March 2020, the first JMA's C-band dual-polarization Doppler radar for disaster prevention was deployed in Kashiwa City. The same series of the other radars are sequentially replaced by dual-polarization radar. In addition, data from the dual-polarization Doppler radars for airport weather already in operation at Haneda and Narita airports can be used, as in this study. The JMA's wind profiler radar observations are made at the Katsuura, Kumagaya, Mito, and Kawaguchiko observational sites in the Kanto region.

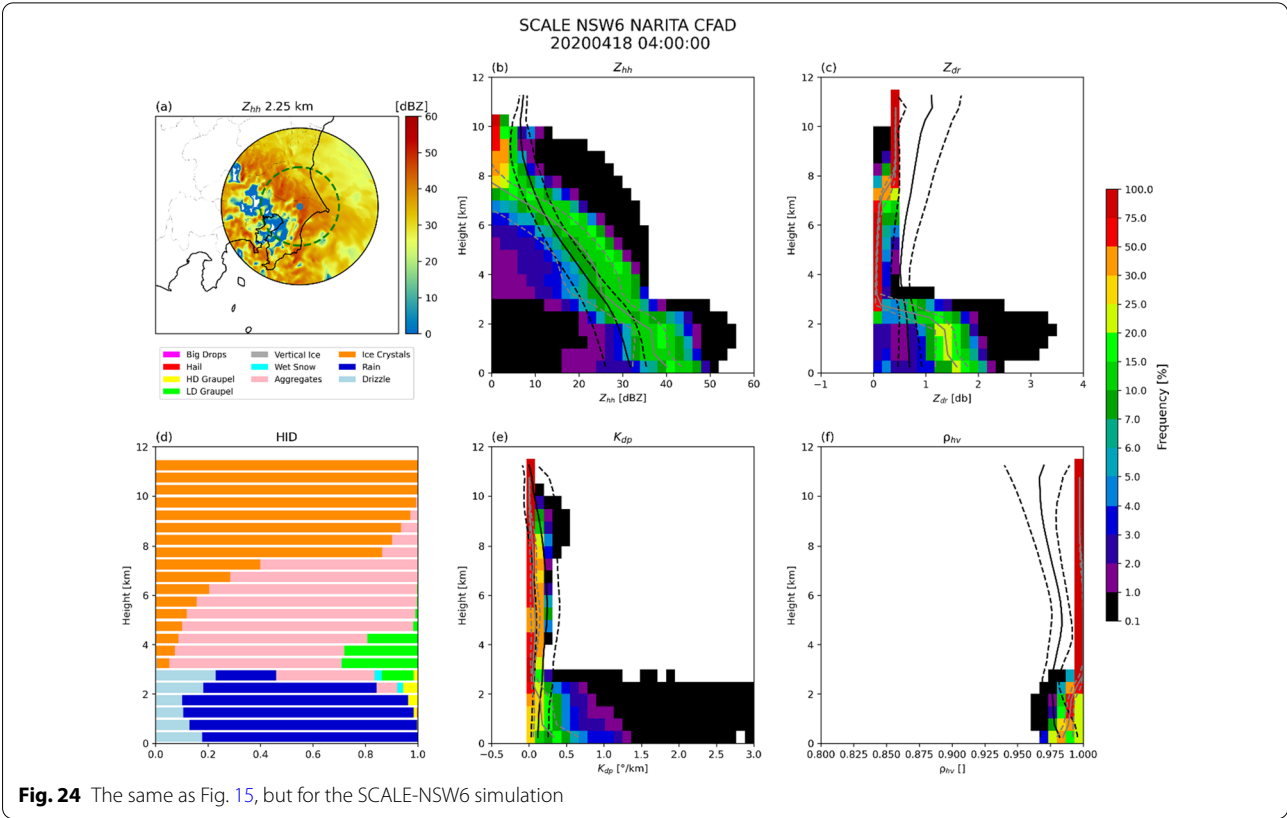
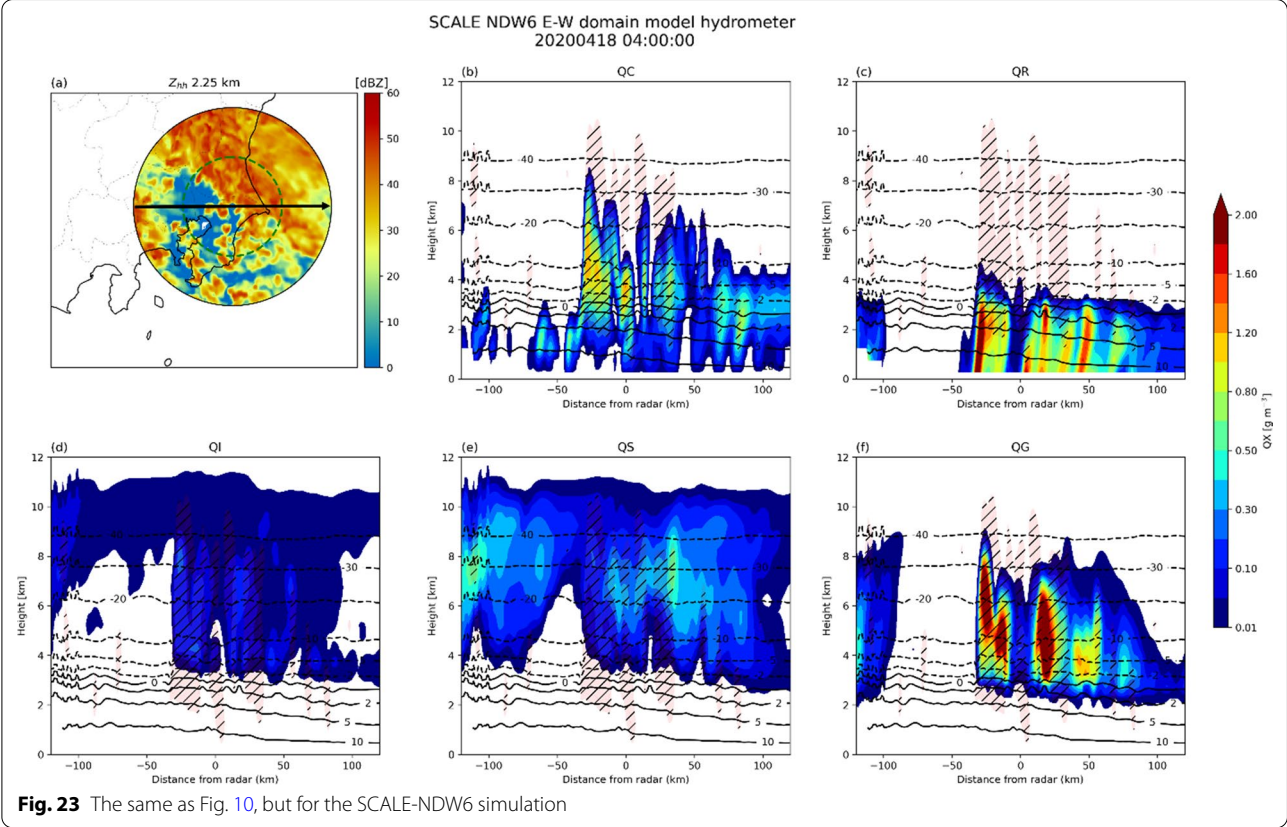
Appendix 2: Analysis of the experiments with SCALE

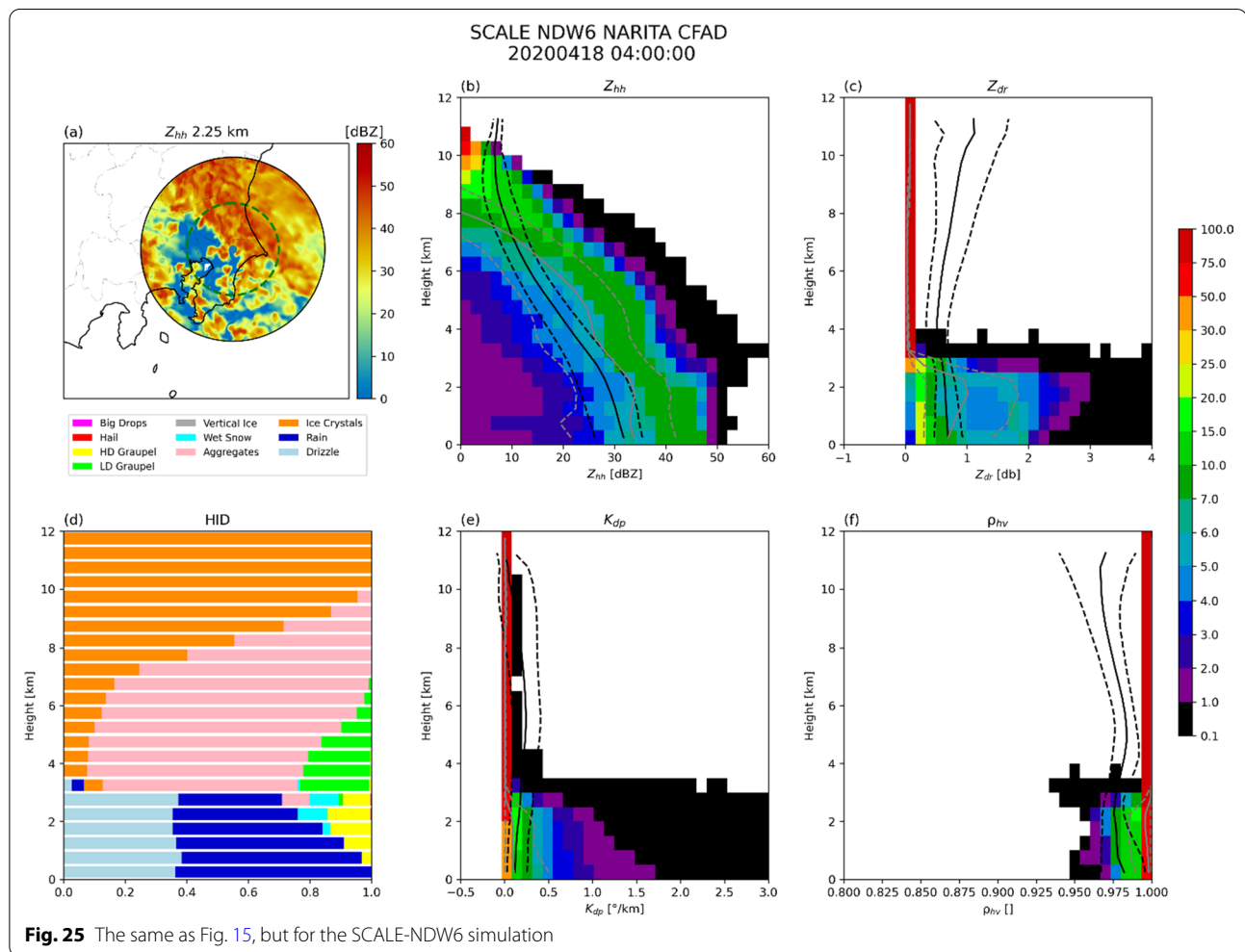
Figures 20, 21, 22, 23, 24, and 25 show the analysis of the experiments with SCALE. The cross sections of the distribution of polarimetric parameters and hydrometeors of the SCALE-NSW6 experiment are shown in Figs. 20, 21, and those of the SCALE-NDW6 experiment are shown in Figs. 22, 23. The CFADs of the polarimetric parameters of the SCALE-NSW6 experiment are shown in Fig. 24, and those of the SCALE-NDW6 experiment are shown in Fig. 25.

One of the major differences between NICAM and SCALE is that of the storm top height: Figs. 10, 11 vs. Figs. 21, 23. For example, SCALE shows the snow height is higher than NICAM. We found that this difference in snow comes from the upward motions. The frequency distribution of upwelling is stronger for SCALE than for NICAM in the middle of the troposphere (not shown), although the CFADs for Z_{hh} are not significantly different (Figs. 15b, 16b vs. Figs. 24b, 25b). Overall, we interpret these results as there is not much difference in microphysics reproducibility if we consider the difference between the dynamical core and the initial condition.









Abbreviations

ASUCA: A System based on a Unified Concept for Atmosphere; DM: Double moment; DYAMOND: Dynamics of the Atmospheric general circulation Modeled on Non-hydrostatic Domains; GCM: General circulation model; GSRM: Global storm-resolving model; HID: Hydrometeor Identification; JMA: Japan Meteorological Agency; J-Sim: Joint Simulator for Satellite Sensors; MCS: Mesoscale convective system; NICAM: Non-hydrostatic ICosahedral Atmospheric Model; NDW6: NICAM double-moment bulk cloud microphysics with six water categories; NSW6: NICAM single-moment bulk cloud microphysics with six water categories; POLARRIS: POLARimetric Radar Retrieval and Instrument Simulator; PPI: Plan position indicator; RHI: Range–Height Indicator; SCALE: Scalable Computing for Advanced Library and Environment; SM: Single moment; ULTIMATE: ULtra-slte for Measuring Atmosphere of Tokyo metropolitan Environment.

Acknowledgements

The Meteorological Research Institute provided the data of the dual-polarization Doppler radar for airport weather. The cooperation of the Japan Meteorological Agency made it possible for the authors to use the regional model ASUCA. The regional model SCALE was obtained from RIKEN (<https://scale.riken.jp/ja/>), and CSU Radar Tools is available at https://github.com/CSU-Radar-met/CSU_RadarTools. JAXA supports the scientific research of the EarthCARE mission. This work was supported by the Japan Society for the Promotion of Science, KAKENHI, Grant-in-Aid for Scientific Research B (20H01967) for ULtra-slte for Measuring Atmosphere of Tokyo Metropolitan Environment and Collaboration Studies with High-Resolution Atmospheric Models (ULTIMATE), and

by the Program for Promoting Technological Development of Transportation (Ministry of Land, Infrastructure, Transport and Tourism of Japan). The computational resources were provided by the National Institute for Environmental Studies. This work was partly supported by the joint research program of the Institute for Space-Earth Environmental Research (ISEE), Nagoya University. The authors appreciate Dr. Akihito Umehara for giving information on the description of the dual-polarization Doppler radar for airport weather and for improving the manuscript.

Author contributions

MS proposed the topic and led ULTIMATE. SM conducted all the numerical simulations. WR and YI investigated the cloud microphysics characteristics of NICAM and ASUCA, respectively. NK contributed to summarizing the results. TS contributed to the analysis of cloud microphysics schemes, particularly NDW6. TH developed the Joint Simulator for Satellite Sensors and implemented POLARRIS. HO contributed to the observation of the ground validation of EarthCARE. All authors read and approved the final manuscript.

Funding

This research is part of the EarthCARE satellite study commissioned by the Japan Aerospace Exploration Agency, “Enhancement of the Joint Simulator for Satellite Sensors,” and the Grant-in-Aid for Scientific Research B “Promotion of Collaborative Research on High-Resolution Numerical Models through Comprehensive Use of Ultrasite Observations in the Kanto Region” (20H01967). Program for Promoting Technological Development of Transportation of the Ministry of Land, Infrastructure, Transport and Tourism (MLIT) supported the

research “Advancement of Extreme Weather Prediction for Efficient Operation of Aircraft in the Kanto Region.” This work was carried out as part of the joint research program of the Institute for Space-Earth Environmental Research (ISEE), Nagoya University. We also acknowledge the National Institute for Environmental Studies (NIES) granting us permission to use their supercomputer system (NEC SX-ACE/128M16, NEC SX-Aurora TSUBASA A511-64).

Availability of data and materials

The numerical model SCALE is available at <https://scale.riken.jp/>; NICAM is available on request, as described at <http://nicam.jp/hiki/?Research+Collaborations>. Those interested in the availability of the numerical model “ASUCA” should contact the first author (MS). The Joint Simulator for Satellite Sensors is described at https://www.eorc.jaxa.jp/theme/Joint-Simulator/userform/js_userform.html. The numerical data from the present study are available on request from the first author (MS).

Declarations

Competing interests

The authors declare that they have no competing interests.

Author details

¹Atmosphere and Ocean Research Institute, The University of Tokyo, 5-1-5 Kashiwanoha, Kashiwa, Chiba 277-8564, Japan. ²Meteorological Research Institute, Japan Meteorological Agency, Tsukuba, Japan. ³Japan Agency for Marine-Earth Science and Technology, Yokohama, Japan. ⁴Kochi University of Technology, Kochi, Japan. ⁵Research Institute for Applied Mechanics, Kyushu University, Fukuoka, Japan.

Received: 25 March 2022 Accepted: 26 September 2022

Published online: 12 October 2022

References

- Bodas-Salcedo A, Webb MJ, Bony S, Chepfer H, Dufresne JL, Klein SA et al (2011) COSP: Satellite simulation software for model assessment. *Bull Am Meteorol Soc* 92:1023–1043. <https://doi.org/10.1175/2011BAMS2856.1>
- Bringi V, Seifert A, Wu W, Thurai M, Huang GJ, Siewert C (2020) Hurricane Dorian outer rain band observations and 1d particle model simulations: a case study. *Atmosphere (basel)* 11:879. <https://doi.org/10.3390/ATMOS11080879>
- Dolan B, Rutledge SA (2009) A theory-based hydrometeor identification algorithm for X-band polarimetric radars. *J Atmos Ocean Technol* 26:2071–2088. <https://doi.org/10.1175/2009JTECHA1208.1>
- Dolan B, Rutledge SA, Lim S, Chandrasekar V, Thurai M (2013) A robust C-band hydrometeor identification algorithm and application to a long-term polarimetric radar dataset. *J Appl Meteorol Climatol* 52:2162–2186. <https://doi.org/10.1175/JAMC-D-12-0275.1>
- Eyring V, Bony S, Meehl GA, Senior CA, Stevens B, Stouffer RJ et al (2016) Overview of the Coupled Model Intercomparison Project Phase 6 (CMIP6) experimental design and organization. *Geosci Model Dev* 9:9. <https://doi.org/10.5194/gmd-9-1937-2016>
- Haarsma RJ, Roberts M, Vidale PL, Senior C, Bellucci A, Corti S, Fuckar N, Gue-mas V, von Hardenberg J, Hazeleger W, Kodama C, Koenig T, Leung R, Lu J, Luo J-J, Mao J, Mizielinsky M, Mizuta R, Nobre P, Sato M, Scoc-cimarro E, Semmler T, Small J, von Storch J-S (2016) High resolution model intercomparison project (HighResMIP v1.0) for CMIP6. *Geosci Model Dev* 9:4185–4208. <https://doi.org/10.5194/gmd-2016-66>
- Harris L, Zhou L, Lin S-J, Chen J-H, Chen X, Gao K et al (2020) GFDL SHIELD: a unified system for weather-to-seasonal prediction. *J. Adv. Model. Earth Syst.* 12:e2020MS002223. <https://doi.org/10.1029/2020MS002223>
- Hashino T, Sato M, Hagihara Y, Kubota T, Matsui T, Nasuno T, Okamoto H (2013) Evaluating cloud microphysics from the NICAM against Cloud-Sat and CALIPSO. *J Geophys Res* 118:7273–7293. <https://doi.org/10.1002/jgrd.50564>
- Hashino T, Sato M, Hagihara Y, Kato S, Kubota T, Matsui T, Nasuno T, Okamoto H, Sekiguchi M (2016) Evaluating cloud radiative effects simulated by NICAM with A-train. *J Geophys Res* 121:7041–7063. <https://doi.org/10.1002/2016JD024775>
- Helmus JJ, Collis SM (2016) The Python ARM Radar Toolkit (Py-ART), a library for working with weather radar data in the python programming language. *J Open Res Software* 4:e25. <https://doi.org/10.5334/jors.119>
- Hersbach H, Bell B, Berrisford P, Hirahara S, Horányi A, Muñoz-Sabater J et al (2020) The ERA5 global reanalysis. *Q J R Meteorol Soc* 146:1999–2049. <https://doi.org/10.1002/QJ.3803>
- Ikuta Y, Sato M, Sawada M, Kusabiraki H, Kubota T (2021) Improvement of the cloud microphysics scheme of the mesoscale model at the Japan Meteorological Agency using space-borne radar and microwave Imager of the Global Precipitation Measurement as reference. *Mon Wea Rev* 149:3803–3819. <https://doi.org/10.1175/MWR-D-21-0066.1>
- Ikuta Y, Sawada M, Sato M (2022) Determining the impact of boundary layer schemes on the secondary circulation of Typhoon FAXAI using radar observations in the gray zone. *J Atmos Sci* (submitted)
- Illingworth A, Barker H, Beljaars A, Ceccaldi M, Chepfer H, Delanoe J, Dome-nech C, Donovan D, Fukuda S, Hirakata M, Hogan R, Huenerbein A, Kollias P, Kubota T, Nakajima T, Nakajima T, Nishizawa T, Ohno Y, Okamoto H, Oki R, Sato K, Sato M, Wandinger U, Wehr T (2015) The EARTHCARE satellite: the next step forward in global measurements of clouds, aerosols, precipitation and radiation. *Bull Am Meteorol Soc* 96:1311–1332
- Japan Meteorological Agency (2019) Outline of the operational numerical weather prediction at the Japan Meteorological Agency, Appendix to WMO technical progress report on the global data-processing and forecasting system and numerical weather prediction. 229 pp. <https://www.jma.go.jp/jma/eng/jma-center/nwp/outline2019-nwp/index.htm>
- Jung Y, Xue M, Zhang G (2010) Simulations of polarimetric radar signatures of a supercell storm using a two-moment bulk microphysics scheme. *J Appl Meteorol Climatol* 49:146–163. <https://doi.org/10.1175/2009JAMC2178.1>
- Karrer M, Seifert A, Ori D, Kneifel S (2021) Improving the representation of aggregation in a two-moment microphysical scheme with statistics of multi-frequency Doppler radar observations. *Atmos Chem Phys* 21:17133–17166. <https://doi.org/10.5194/acp-21-17133-2021>
- Khairoutdinov MF, Blossey PN, Bretherton CS (2022) Global system for atmospheric modeling: model description and preliminary results. *J Adv Model Earth Syst* 14:e2021MS002968. <https://doi.org/10.1029/2021MS002968>
- Kodama C, Noda AT, Sato M (2012) An assessment of the cloud signals simulated by NICAM using ISCCP, CALIPSO, and CloudSat satellite simulators. *J Geophys Res* 117:D12210. <https://doi.org/10.1029/2011JD017317>
- Kodama C, Ohno T, Seiki T, Yashiro H, Noda AT, Nakano M, Yamada Y, Roh W, Sato M, Nitta T, Goto D, Miura H, Nasuno T, Miyakawa T, Chen Y-W, Sugi M (2021) The non-hydrostatic global atmospheric model for CMIP6 High-ResMIP simulations (NICAM16-S): experimental design, model description, and sensitivity experiments. *Geosci Model Dev* 14:795–820
- Masunaga H, Sato M, Miura H (2008) A joint satellite and global CRM analysis of an MJO event: model diagnosis. *J Geophys Res* 113:D17210. <https://doi.org/10.1029/2008JD009986>
- Masunaga H, Matsui T, Tao WK, Hou AY, Kummerow CD, Nakajima T et al (2010) Satellite data simulator unit: a multisensor, multispectral satellite simulator package. *Bull Am Meteorol Soc* 91:1625–1632. <https://doi.org/10.1175/2010BAMS2809.1>
- Matsui T, Tao WK, Munchak SJ, Grecu M, Huffman GJ (2015) Satellite view of quasi-equilibrium states in tropical convection and precipitation microphysics. *Geophys Res Lett* 42:1959–1968. <https://doi.org/10.1002/2015GL063261>
- Matsui T, Tao W-K, Chern J, Lang S, Sato M, Hashino T, Kubota T (2016) On the land-ocean contrast of tropical convection and microphysics statistics derived from TRMM satellite signals and global storm-resolving models. *J Hydrometeorol* 17:1425–1445. <https://doi.org/10.1175/JHM-D-15-0111.1>
- Matsui T, Wolff DB, Mohr KI, Lang SE, Zhang M (2019a) Bilateral operational storm-scale observation and modeling: BLOSSOM. American Geophysical Union, Fall Meeting 2019a, abstract #H31P-1980, December 2019, 2019aAGUFM.H31P1980M.
- Matsui T, Dolan B, Rutledge SA, Tao WK, Iguchi T, Barnum J, Lang SE (2019b) POLARRIS: A POLArimetric radar retrieval and instrument simulator. *J Geophys Res Atmos* 124:4634–4657
- Matsui T, Dolan B, Iguchi T, Rutledge SA, Tao W-K, Lang S (2020) Polarimetric radar characteristics of simulated and observed intense convective

- cores for a midlatitude continental and tropical maritime environment. *J Hydrometeorol* 21:501–517
- Misumi R (2018) Preface. Special Issue on Tokyo Metropolitan Area Convection Study for Extreme Weather Resilient Cities (TOMACS). *J Meteor Soc Japan* 96A:1–2
- Misumi R, Shoji Y, Saito K, Seko H, Seino N, Suzuki S et al (2019) Results of the Tokyo Metropolitan Area Convection Study for Extreme Weather Resilient Cities (TOMACS). *Bull Am Meteorol Soc* 100:2027–2041. <https://doi.org/10.1175/BAMS-D-18-0316.1>
- Miyoshi T, Sato S, Ushio T, Koike K, Park T, Nakajima K (2020) Guerrilla rainfall forecast updated every 30 seconds—Real-time demonstration in the Tokyo metropolitan area. https://www.riken.jp/pr/news/2020/20200821_1/index.html. Accessed April 17, 2021
- Nishizawa S, Yashiro H, Sato Y, Miyamoto Y, Tomita H (2015) Influence of grid aspect ratio on planetary boundary layer turbulence in large-eddy simulations. *Geosci Model Dev* 8:3393–3419
- Noda AT, Seiki T, Roh W, Satoh M, Ohno T (2021) Improved representation of low-level mixed-phase clouds in a global cloud-system-resolving simulation. *J Geophys Res Atmosphere* 126:e2021JD035223. <https://doi.org/10.1029/2021JD035223>
- Putnam BJ, Xue M, Jung Y, Zhang G, Kong F (2017) Simulation of polarimetric radar variables from 2013 CAPS spring experiment storm-scale ensemble forecasts and evaluation of microphysics schemes. *Mon Wea Rev* 145:49–73. <https://doi.org/10.1175/MWR-D-15-0415.1>
- Roh W, Satoh M (2014) Evaluation of precipitating hydrometeor parameterizations in a single-moment bulk microphysics scheme for deep convective systems over the tropical open ocean. *J Atmos Sci* 71:2654–2673
- Roh W, Satoh M (2018) Extension of a multisensor satellite radiance-based evaluation for cloud system resolving models. *J Meteor Soc Japan* 96:55–63
- Roh W, Satoh M, Nasuno T (2017) Improvement of a cloud microphysics scheme for a global nonhydrostatic model using TRMM and a satellite simulator. *J Atmos Sci* 74:167–184
- Roh W, Satoh M, Hashino T, Okamoto H, Seiki T (2020) Evaluations of the thermodynamic phases of clouds in a cloud system-resolving model using CALIPSO and a satellite simulator over the Southern Ocean. *J Atmos Sci* 77:3781–3801
- Roh W, Satoh M, Hohenegger C (2021) Intercomparison of cloud properties in DYAMOND simulations over the Atlantic Ocean. *J Meteor Soc Japan* 99:1439–1451
- Ryzhkov A, Pinsky M, Pokrovsky A, Khain A (2011) Polarimetric radar observation operator for a cloud model with spectral microphysics. *J Appl Meteorol Climatol* 50:873–894. <https://doi.org/10.1175/2010JAMC2363.1>
- Sato Y, Nishizawa S, Yashiro H, Miyamoto Y, Kajikawa Y, Tomita H (2015) Impacts of cloud microphysics on trade wind cumulus: which cloud microphysics processes contribute to the diversity in a large eddy simulation. *Prog Earth Planet Sci* 2:23
- Satoh M, Matsuno T, Tomita H, Miura H, Nasuno T, Iga S (2008) Nonhydrostatic Icosahedral Atmospheric Model (NICAM) for global cloud resolving simulations. *J Comp Phys* 227:3486–3514. <https://doi.org/10.1016/j.jcp.2007.02.006>
- Satoh M, Inoue T, Miura H (2010) Evaluations of cloud properties of global and local cloud system resolving models using CALIPSO/CloudSat simulators. *J Geophys Res* 115:D00H14. <https://doi.org/10.1029/2009JD012247>
- Satoh M, Tomita H, Yashiro H, Miura H, Kodama C, Seiki T, Noda AT, Yamada Y, Goto D, Sawada M, Miyoshi T, Niwa Y, Hara M, Ohno Y, Iga S, Arakawa T, Inoue T, Kubokawa H (2014) The non-hydrostatic icosahedral atmospheric model: description and development. *Prog Earth Planet Sci* 1:18
- Satoh M, Roh W, Hashino T (2016) Evaluations of clouds and precipitations in NICAM using the Joint Simulator for Satellite Sensors. Cger's Supercomputer Monograph Report 22:110
- Satoh M, Noda AT, Seiki T, Chen Y-W, Kodama C, Yamada Y, Kuba N, Sato Y (2018) Toward reduction of the uncertainties in climate sensitivity due to cloud processes using a global non-hydrostatic atmospheric model. *Prog Earth Planet Sci* 5:67. <https://doi.org/10.1186/s40645-018-0226-1>
- Satoh M, Stevens B, Judt F, Khairoutdinov M, Lin S, Putman WM (2019) Global cloud-resolving models. *Curr Clim Chang Rep* 5:172–184. <https://doi.org/10.1007/s40641-019-00131-0>
- Seiki T, Nakajima T (2014) Aerosol effects of the condensation process on a convective cloud simulation. *J Atmos Sci* 71:833–853
- Seiki T, Roh W (2020) Improvements in supercooled liquid water simulations of low-level mixed-phase clouds over the Southern Ocean using a single-column model. *J Atmos Sci* 77:3803–3819
- Seiki T, Satoh M, Tomita H, Nakajima T (2014) Simultaneous evaluation of ice cloud microphysics and non-sphericity of the cloud optical properties using hydrometeor video sonde and radiometer sonde in-situ observations. *J Geophys Res Atmos* 119:6681–6701
- Seiki T, Kodama C, Satoh M, Hashino T, Hagihara Y, Okamoto H (2015) Vertical grid spacing necessary for simulating tropical cirrus clouds with a high-resolution atmospheric general circulation model. *Geophys Res Lett* 42:4150–4157
- Sherwood SC, Webb MJ, Annan JD, Armour KC, Forster PM, Hargreaves JC et al (2020) An assessment of earth's climate sensitivity using multiple lines of evidence. *Rev Geophys* 58:1–92
- Shrestha P, Mendrok J, Pejic V, Trömel S, Blahak U, Carlin JT (2022) Evaluation of the COSMO model (v5.1) in polarimetric radar space—impact of uncertainties in model microphysics, retrievals and forward operators. *Geosci Model Dev* 15:291–313. <https://doi.org/10.5194/gmd-15-291-2022>
- Skamarock WC, Klemp JB, Duda MG, Fowler LD, Park SH, Ringler TD (2012) A multiscale nonhydrostatic atmospheric model using centroidal Voronoi tessellations and C-grid staggering. *Mon Weather Rev* 140:3090–3105. <https://doi.org/10.1175/MWR-D-11-00215.1>
- Snyder JC, Bluestein HB, Dawson DT, Jung Y (2017a) Simulations of polarimetric, X-band radar signatures in supercells. Part I: description of experiment and simulated ρ_{hv} rings. *J Appl Meteorol Climatol* 56:1977–1999. <https://doi.org/10.1175/JAMC-D-16-0138.1>
- Snyder JC, Bluestein HB, Dawson DT, Jung Y (2017b) Simulations of polarimetric, X-band radar signatures in supercells. Part II: Z_{DR} columns and rings and K_{DP} columns. *J Appl Meteorol Climatol* 56:2001–2026. <https://doi.org/10.1175/JAMC-D-16-0139.1>
- Stevens B, Satoh M, Auger L, Biercamp J, Bretherton C, Chen X, Duben P, Judt F, Khairoutdinov M, Klocke D, Kodama C, Kornblueh L, Lin S-L, Putman W, Shibuya R, Neumann P, Rober N, Vannier B, Vidale P-L, Wedi N, Zhou L (2019) DYAMOND: the dynamics of the atmospheric general circulation modeled on non-hydrostatic domains. *Prog Earth Planet Sci* 6:61. <https://doi.org/10.1186/s40645-019-0304-z>
- Tomita H (2008) A stretched grid on a sphere by new grid transformation. *J Meteor Soc Japan* 86A:107–119
- Tomita H, Tsugawa M, Satoh M, Goto K (2001) Shallow water model on a modified icosahedral geodesic grid by using spring dynamics. *J Comput Phys* 174:579–613. <https://doi.org/10.1006/jcp.2001.6897>
- Tomita H, Satoh M (2004) A new dynamical framework of nonhydrostatic global model using the icosahedral grid. *Fluid Dyn Res* 34:357–400
- Trömel S, Simmer C, Blahak U, Blanke A, Doktorowski S, Ewald F et al (2021) Overview: fusion of radar polarimetry and numerical atmospheric modeling towards an improved understanding of cloud and precipitation processes. *Atmos Chem Phys* 21:17291–17314. <https://doi.org/10.5194/acp-21-17291-2021>
- Tsukamoto N, Yamauchi H, Okumura H, Umehara A, Kajiwara Y (2016) JMA's C-band dual-polarization Doppler weather radars with SSPAs. WMO Technical Conference on Meteorological and Environmental Instruments and Methods of Observation 2016, Madrid, Spain, 27–29 September 2016. Available online at: [https://www.wmo.net/eventpapers/session2/posters/P2\(68\)%20Tsukamoto_JMA-radars.pdf](https://www.wmo.net/eventpapers/session2/posters/P2(68)%20Tsukamoto_JMA-radars.pdf). accessed 04 August 2022
- Uchida J, Mori M, Nakamura H, Satoh M, Suzuki K, Nakajima T (2016) Error and energy budget analysis of a nonhydrostatic stretched-grid global atmospheric model. *Mon Wea Rev* 144:1423–1447
- Uchida J, Mori M, Hara M, Satoh M, Goto D, Kataoka T, Suzuki K, Nakajima T (2017) Impact of lateral boundary errors on the simulation of clouds with a non-hydrostatic regional climate model. *Mon Wea Rev* 145:5059–5082
- Umehara A, Adachi T, Mashiko W, Yamauchi H (2021) Analysis of the tornadic debris signatures of the Ichihara Tornado in a typhoon environment using two operational C-band dual-polarization weather radars. *SOLA* 17:196–201. <https://doi.org/10.2151/SOLA.2021-034>
- Webb MJ, Andrews T, Bodas-Salcedo A, Bony S, Bretherton CS, Chadwick R et al (2017) The cloud feedback model intercomparison project (CFMIP) contribution to CMIP6. *Geosci Model Dev* 10:359–384. <https://doi.org/10.5194/gmd-10-359-2017>

Zängl G, Reinert D, Rípodas P, Baldauf M (2014) The ICON (ICOsahedral Non-hydrostatic) modelling framework of DWD and MPI-M: Description of the non-hydrostatic dynamical core. *Q J R Meteorol Soc* 141:563–579. <https://doi.org/10.1002/qj.2378>

Publisher's Note

Springer Nature remains neutral with regard to jurisdictional claims in published maps and institutional affiliations.

Submit your manuscript to a SpringerOpen[®] journal and benefit from:

- Convenient online submission
- Rigorous peer review
- Open access: articles freely available online
- High visibility within the field
- Retaining the copyright to your article

Submit your next manuscript at ► [springeropen.com](https://www.springeropen.com)
